Journal of Volcanology and Geothermal Research 351 (2018) 115–133

Contents lists available at ScienceDirect

Journal of Volcanology and Geothermal Research

journal homepage: www.elsevier.com/locate/jvolgeores

Geological evolution of the Boset-Bericha Volcanic Complex, Main Ethiopian Rift: $^{40}Ar/^{39}Ar$ evidence for episodic Pleistocene to Holocene volcanism

Melanie Siegburg [a,*], Thomas M. Gernon [a], Jonathan M. Bull [a], Derek Keir [a,b], Dan N. Barfod [c], Rex N. Taylor [a], Bekele Abebe [d], Atalay Ayele [e]

[a] School of Ocean and Earth Science, National Oceanography Centre Southampton, University of Southampton, European Way, Southampton SO14 3ZH, UK
[b] Dipartimento di Scienze della Terra, Universita degli Studi di Firenze, Florence 50121, Italy
[c] Argon Isotope Facility, Scottish Universities Environmental Research Centre, Rankine Avenue, Scottish Enterprise Technology Park, East Kilbride G75 0QF, UK
[d] Department of Earth Sciences, Addis Ababa University, P.O. Box 1176, Addis Ababa, Ethiopia
[e] Institute of Geophysics, Space Science and Astronomy, Addis Ababa University, Addis Ababa, Ethiopia

ARTICLE INFO

Article history:
Received 8 October 2017
Received in revised form 14 December 2017
Accepted 19 December 2017
Available online 29 December 2017

Keywords:
Episodic volcanism
Continental rifting
$^{40}Ar/^{39}Ar$ geochronology
Main Ethiopian Rift
Peralkaline

ABSTRACT

The Boset-Bericha Volcanic Complex (BBVC) is one of the largest stratovolcanoes of the northern Main Ethiopian Rift (MER). However, very little is known about its eruptive history, despite the fact that approximately 4 million people live within 100 km of the complex. Here, we combine field observations, morphometric analysis using high-resolution LiDAR data, geochemistry and $^{40}Ar/^{39}Ar$ geochronology to report the first detailed account of the geological evolution of the BBVC, with a focus on extensive young lava flows covering the two edifices, Gudda and Bericha. These lavas exhibit a bimodal composition ranging dominantly from basaltic rift floor lavas and scoria cones, to pantelleritic trachytes and rhyolite flows at Gudda, and comenditic rhyolites at Bericha. Further, several intermediate compositions are associated with fissure vents along the Boset-Kone segment that also appear to link the silicic centres. We divide the BBVC broadly into four main eruptive stages, comprising: (1) early rift floor emplacement, (2) formation of Gudda Volcano within two main cycles, separated by caldera formation, (3) formation of the Bericha Volcano, and (4) sporadic fissure eruptions. Our new $^{40}Ar/^{39}Ar$ geochronology, targeting a representative array of these flows, provides evidence for episodic activity at the BBVC from ~120 ka to the present-day. We find that low-volume mafic episodes are more frequent (~10 ka cyclicity) than felsic episodes (~100 ka cyclicity), but the latter are more voluminous. Over the last ~30 ka, mafic to intermediate fissure activity might have reinvigorated felsic activity (over the last ~16 ka), manifested as peralkaline lava flows and pyroclastic deposits at Gudda and Bericha. Felsic episodes have on average a higher eruption rate (2–5/1000 years) and productivity at Gudda compared to Bericha (1–2/1000 years). The young age of lavas and current fumarolic activity along the fault system, suggest that the BBVC is still potentially active. Coincident episodic activity within the BBVC and at several rift segments in the MER is observed, and facilitates continental rifting.

1. Introduction

Volcanism in Ethiopia is thought to have commenced at ~60 Ma with a strong pulse of flood basalt activity around ~28–31 Ma associated with the Afar Plume (Hofmann et al., 1997). The flood basalts are approximately coeval with initiation of rifting in the Red Sea and Gulf of Aden, whereas rifting started around 11 Ma in the northern part of the MER (WoldeGabriel et al., 1990; Wolfenden et al., 2004). Time constraints of Quaternary volcanism within the northern Main Ethiopian Rift (MER) (Fig. 1) are rare and mainly developed in the context of early hominid evolution (Vogel et al., 2006; Morgan and Renne, 2008; Sahle et al., 2013, 2014; Hutchison et al., 2016a). Two main Quaternary silicic-centre volcanic episodes occurred in the rift between 2 and 1 Ma with basaltic flows followed by ignimbrites, while activity in the last ~0.65 Ma was dominated by axial silicic volcanoes and basalts (Chernet et al., 1998; Abebe et al., 2007). Absolute dates of fault activity (WoldeGabriel et al., 1990; Chernet et al., 1998; Boccaletti et al., 1999; Wolfenden et al., 2004) and eruptive phases of Quaternary volcanoes throughout the northern MER (Harris, 1844; Cole, 1969; Di Paola, 1972; Bigazzi et al., 1993; Peccerillo et al., 2003; Williams et al., 2004; Hutchison et al., 2016b; Rapprich et al., 2016) are scattered and at a regional scale. Further, detailed age control from high resolution studies to constrain the evolution of individual volcanic complexes is rare and until now only constrained for Aluto Volcano (Hutchison et al., 2016b). Such constraints are vital to understand the role of magmatism within individual volcanic complexes though time during continental rifting.

* Corresponding author.
E-mail address: ms1f14@soton.ac.uk (M. Siegburg).

https://doi.org/10.1016/j.jvolgeores.2017.12.014

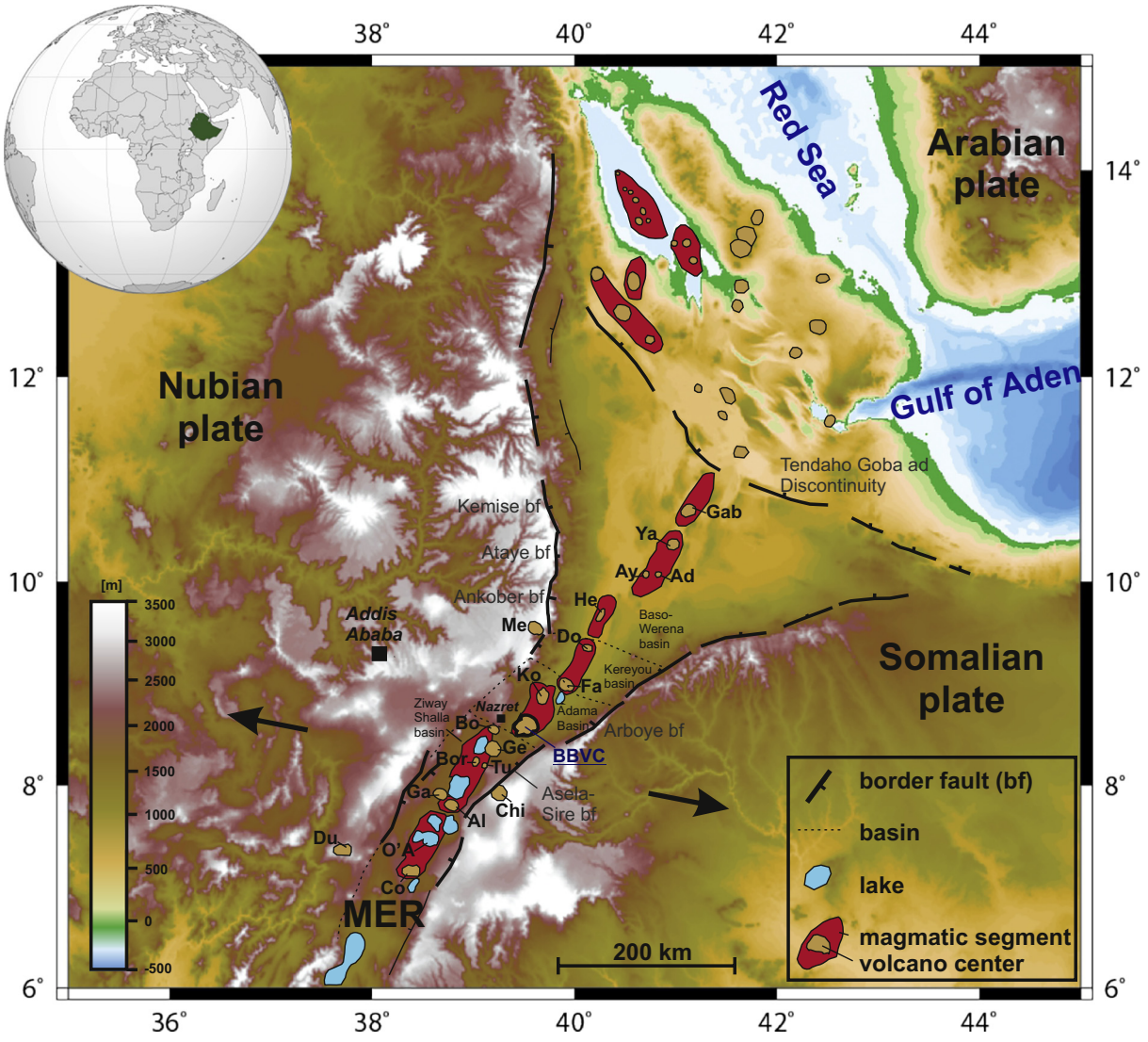

Fig. 1. Map of the Main Ethiopian Rift formed by rifting of the Nubian and Somalian plate. Magmatic segments are red with silicic centres in brown. The BBVC is located between Kone and Gedemsa Caldera in the Adama basin. Further silicic centres are mapped from south to north, Corbetti (Co), Dunguna (Du), O'a caldera (O'a), Aluto (Al), Gademotta (Ga), Chilalo (Chi), Bora Bericha (Bor), Tulu Moye (Tu), Gedemsa (Ge), Boku (Bo), Kone (Ko), Fantale (Fe), Dofen (Do), Megezez (Me), Hertali (He), Ayelu (Ay), Adwa (Ad), Yangudi (Ya), Gabillema (Gab).

The focus of this study is one of the largest stratovolcanoes in the northern MER, the Boset-Bericha Volcanic Complex (BBVC) (Figs. 1, 2). The BBVC was formed by several large silicic explosive and effusive eruptions and comprises the Gudda and Bericha volcanoes. It is associated with several NE-SW orientated fissure systems on the southern end of the Boset-Kone magmatic segment in the Adama basin. The BBVC is broadly divided in having pre- and post-caldera volcanic deposits with a remnant caldera rim on the western side at Gudda, which is dominantly covered by voluminous young post-caldera lavas on the eastern and southern side. This stratovolcano stage of evolution makes the BBVC unique and different to neighbouring volcanoes in the MER, which are typically dominated by calderas. Absolute K/Ar dating of individual cones and flows around the BBVC has been undertaken (Morbidelli et al., 1975; Kazmin et al., 1979; Morton et al., 1979; Chernet et al., 1998; Abebe et al., 2007), but the BBVC has received little attention for a systematic dating of lava flow activity. In particular, only one sample (ignimbrite) from Gudda has been dated and therefore the main part of the BBVC stratovolcano has only been weakly constrained to be around and younger than 1.6 Ma (Morbidelli et al., 1975).

We determine the eruption history of the BBVC for the first time using LiDAR high resolution digital elevation data, supported by Aster, Landsat and satellite images combined with mapping of the relative chronology of different eruption units. The chronology is constrained using observations of lava flow cross-cutting relationships and $^{40}Ar/^{39}Ar$ dates of lava flows. This, together with morphometric, compositional and textural analyses of the lavas provides insights into the style and mode of volcanism throughout the history of the BBVC. Our new absolute chronology allows us to explore recurrence rates of volcanism in the BBVC, and compare how Gudda and Bericha have developed spatially, morphologically and compositionally. This study provides important insights for future volcanic hazard assessments as ~4 million people live within a radius of ~100 km of the BBVC (Aspinall et al., 2011).

2. Geological background

2.1. Main Ethiopian Rift

The Main Ethiopian Rift (MER) is seismically and volcanically active, linking the Afar depression and Kenyan rift in North East Africa (Fig. 1). It is one of a few places worldwide where the transition between continental and oceanic rifting is subaerially exposed. Extension in the northern MER is thought to have started at ~11 Ma (WoldeGabriel et al.,

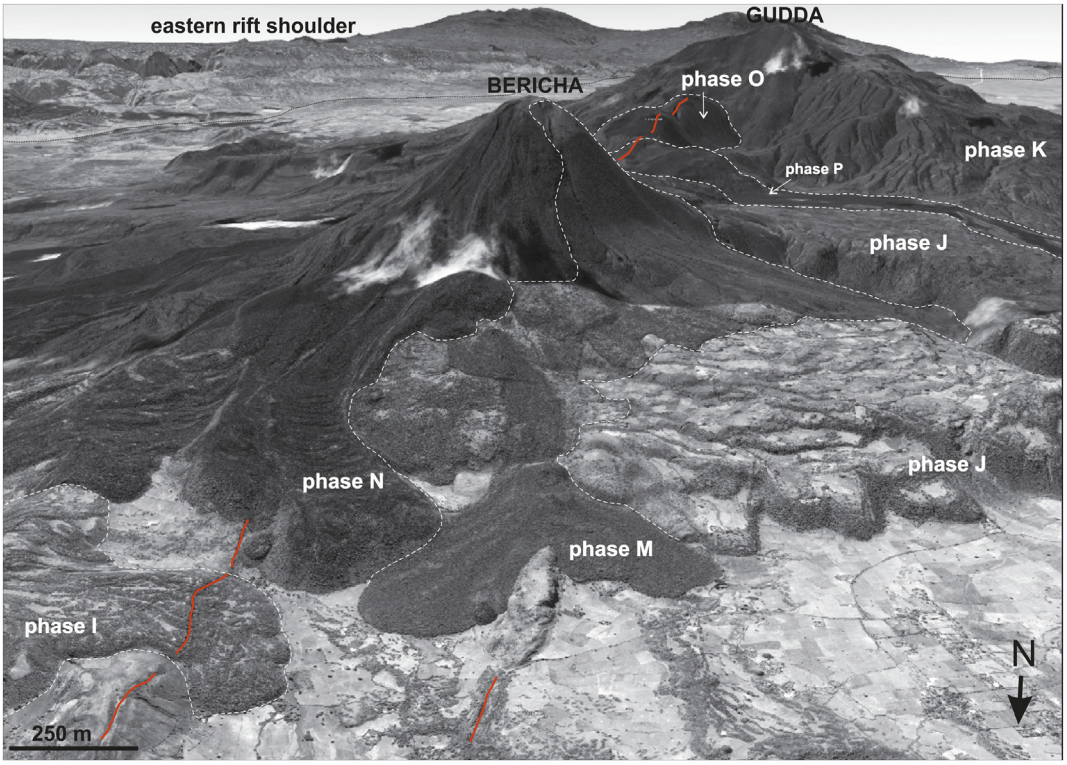

Fig. 2. Oblique satellite view on the BBVC, looking south with 3× vertical exaggeration. Eruption phases are indicated and show the different morphologies as well as compositions (phase J: rhyolite, phase N: obsidian) and flow structures of individual lava flows. Fissures and fractures are along and parallel to the rift axis (red).
(Satellite image from Google Earth.)

1990; Wolfenden et al., 2004) on NE-striking border faults, which define 60–100 km wide grabens (Hayward and Ebinger, 1996). Early rifting was associated with volcanism, mainly near the rift margins (Chernet et al., 1998; Wolfenden et al., 2004; Rooney et al., 2014). Through time, extension and volcanism became focused on the 20-km-wide, right-stepping en-echelon zones of magmatism and faulting (Mohr, 1962, 1967; Ebinger and Casey, 2001; Casey et al., 2006; Keir et al., 2006; Corti, 2009), referred to as "magmatic segments". The morphological expression of these segments is dominated by Quaternary silicic volcanoes (2.6 Ma to present), with aligned monogenetic cones and NNE striking faults and fissures the rift axis (Ebinger and Casey, 2001) (Fig. 1). Extension has been episodic rather than smooth and continuous (Keranen and Klemperer, 2008; Corti, 2009). GPS measurements and plate kinematic modelling suggest extension is still focused on the rift axis and is directed between 095 to 108° from north and at a rate of 4–6 mm per year (Bilham et al., 1999; Fernandes et al., 2004; Bendick et al., 2006; Calais et al., 2006).

The peak in basaltic volcanism (~28 to 31 Ma) (Hofmann et al., 1997; Ukstins et al., 2002; Coulié et al., 2003) was broadly coeval with silicic ignimbrite eruption in the northern MER around 30.2 Ma (Ukstins et al., 2002). The bimodal episode was followed by formation of large basaltic shield volcanoes of transitional to Na-alkaline basalts and minor trachytes in the Miocene (Piccirillo et al., 1979). The next phase of volcanism saw an increase in Miocene activity within the Adama basin including the eruption of Megezez volcano at ~11 Ma (Chernet et al., 1998). Widespread ignimbritic deposits with minor felsic and mafic lavas were emplaced between 6.6 and 5 Ma (WoldeGabriel et al., 1990; Chernet et al., 1998) at the rift margin in the central and northern MER. Magmatism became focused in the rift centre around ~4 Ma to 1 Ma ago (Abebe et al., 2005, 2007; Corti, 2009; Beutel et al., 2010), promoting basaltic eruptions along the Wonji fault belt (e.g. Mohr, 1971), including the Bofa basalt (3.5 to 2.0 Ma (Kazmin et al., 1979); 0.3 Ma (Chernet et al., 1998)). Axial silicic volcanoes and basalts erupted during the last ~650 ka and are dominated by caldera formation events with peralkaline rhyolitic ignimbrites and pumices, ash fall and minor lava flows. Silicic centres became faulted and allowed basalts to erupt through the volcanic edifices and along their flanks (Abebe et al., 2007). The most recent volcanic activity in the northern MER is recorded by historical accounts of fissure basalt flows at Sabober vent south of Fantale volcano between 1770 and 1808 (Harris, 1844), and of the Giano obsidian domes at Tullu Moye Volcano (Di Paola, 1972) indicate very recent volcanism in magmatic segments.

Crustal thickness in this area is constrained from wide-angle seismic refraction and from teleseismic receiver functions and decreases from 38 km in the southern MER beneath the caldera lakes (Fig. 1), to 24 km in the northern MER beneath Fantale volcano (Maguire et al., 2006). The crust of the southeastern plateau is around ~40 km thick, whereas the western plateau of the rift is underlain by ~45–50 km thick crust including a ~10 to 15 km high-velocity lower crust believed to be lower crustal intrusions (Mackenzie et al., 2005). Previous tomographic models (Bastow et al., 2005; Gallacher et al., 2016) indicate that current decompression melting occurs in the asthenosphere at depths of ~70–100 km. Further, Kendall et al. (2005) proposed that partial melt beneath the MER rises through dikes that penetrate the thinned lithosphere and continue into the upper crust (Keir et al., 2005).

2.2. Boset-Bericha Volcanic Complex

The BBVC is located in the northern MER at the southern tip of the NNE-SSW orientated Boset-Kone magmatic segment, 20 km east of Adama/Nazret (Fig. 1). It is one of the largest stratovolcanoes in the MER with a lateral extent of 17 km E-W and 20 km N-S and comprises the northern Bericha Volcano (2120 m) and the southern Gudda Volcano (2447 m) (Fig. 2).

The volcanic history of the BBVC was previously documented by Di Paola (1972) and Brotzu et al. (1974, 1980), whose rock sample data was further analysed by Ronga et al. (2010) and Macdonald et al. (2012). Brotzu et al. (1980) divided the formation of the BBVC into three main phases, 1) pre-caldera activity and formation of the main edifice from "old Gudda Volcano", 2) caldera formation, 3) post-caldera activity, which covers the eastern part of the caldera at the Gudda Volcano and formed the edifice of the Bericha Volcano. The pre-caldera stage in the Pleistocene includes basaltic lava flows, spatter and cinder cones as well as domes and composite cones, and ended with the emplacement of ash and pumice fall deposits. This post-dates the formation of "Balchi-formation" (3.5–1.6 Ma) (Morbidelli et al., 1975; Kazmin et al., 1979; Chernet et al., 1998). "Old Gudda Volcano" is thought to have collapsed during caldera formation on an unknown timescale and post-caldera activity started with thick trachytic pantelleritic lava flows and intercalated pumiceous deposits some time during the Pleistocene–Holocene, on the eastern side of the BBVC. Bericha is thought to have formed at around the same time as Gudda, and involved two central phases and a lateral activity of alkali trachytic rhyolites and comendites (Brotzu et al., 1980). Activity between both edifices is documented as fissure activity sourced from the rift axis and is believed to be younger than the nearby Gara Chisa cone (Morton et al., 1979).

Extension measured by GPS across the Boset-Kone segment (1992–2003), combined with the occurrence of a Mw 5.2 earthquake near the BBVC in 1993 are best explained by dyke intrusion and induced faulting (Bendick et al., 2006). Ongoing seismicity in the EAR is mostly localised in the rift axis above 15 km depth. At the BBVC, however, seismicity is shallower than 8 km (Mazzarini et al., 2013) suggesting heat flow is higher than at other volcanoes in the rift (Beutel et al., 2010). Gravity evidence for a 5 km wide body between 2 and 7.5 km depth directly beneath the BBVC and above the north-western edge of a gabbroic intrusion is interpreted as a distribution of dykes feeding the BBVC from a ca. 8 km deep intrusion (Cornwell et al., 2006; Mickus et al., 2007). At 20 km below surface, high conductivities observed by magnetotellurics suggest a deep zone of partial melt (Whaler and Hautot, 2006). Further the occurrence of a caldera and another shallow conductivity zone (Whaler and Hautot, 2006) suggest a shallow magma storage reservoir (e.g. Ronga et al., 2010). These observations, combined with fumarolic activity and fresh appearance of lava flows suggest the BBVC is active.

3. Methodology

3.1. Field work

Mapping and sampling of the BBVC was undertaken in 2012 and 2015. Fieldwork concentrated on mapping lava flows, ground-truthing remote sensing data (identification of boundaries and sources of different lava flow phases), and mapping of fumarolic activity and fault networks (Figs. 3, 4). Rock specimens (locations shown in Fig. 4) were collected for geochemical and textural analysis as well as radiometric dating using the $^{40}Ar/^{39}Ar$ technique.

3.2. Remote sensing data

Volcano-tectonic mapping at the BBVC integrated observations from remote sensing, in particular LiDAR elevation data, with field observations. High resolution LiDAR data were collected during a NERC ARSF LiDAR survey over BBVC in November 2012 and have 2 m horizontal and 0.2 m vertical resolution. The LiDAR data (Figs. 3, 4) cover the central rift from the edge of the southernmost lava flow of Gudda up to the northern fissure eruption north of Bericha and are recorded within two stripes (30 km long, 5.8 km and 0.75 km width) parallel to the rift axis and one stripe (26.5 km long, 0.75 km width) across the remnant caldera wall of Gudda Volcano. Accuracy of LiDAR data was verified and corrected with GPS stations for ground control points by the Airborne Research and Survey Facility. LiDAR data were combined with more regional Aster data (Fig. 4), to cover the whole volcanic complex. In addition to the digital elevation data, satellite images and Landsat data (multispectral, panchromatic and pansharpened with different resolution and colour bands) were used to identify lava flows, lithology and degree of vegetation.

3.3. Remote sensing methodology - mapping

We mapped different phases of the BBVC as well as individual lava flows, cones and craters, fractures and fissures, topographic features and infrastructure around the BBVC. Geographic Information System (GIS) (UTM, WGS 1984 Zone 37 N) morphometric functions were applied to the LiDAR and Aster data, including *Slope*, *Aspect*, *Curvature*

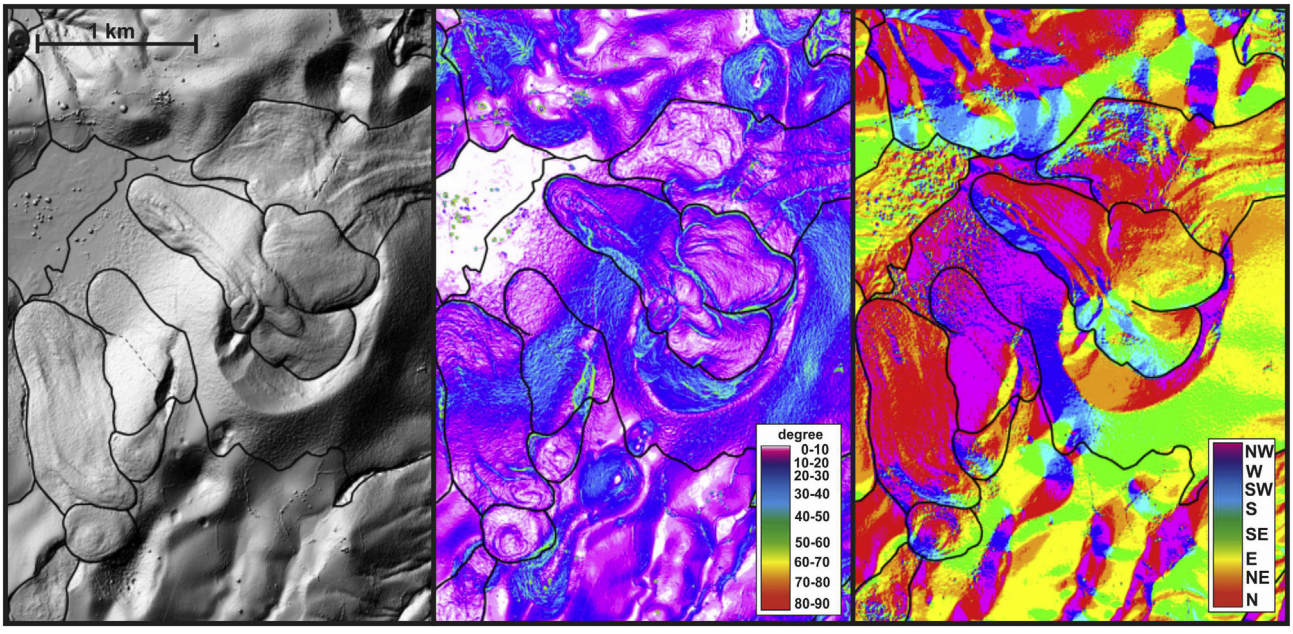

Fig. 3. GIS morphometric tools hillshade, slope and aspect analyses (left to right) were used to map lava flows, cones, craters and tectonic features. The azimuth angle and altitude angle of light source is 315° and 45°, respectively, in the hillshade analysis. The location of the box is shown in Figs. 4 and 5.

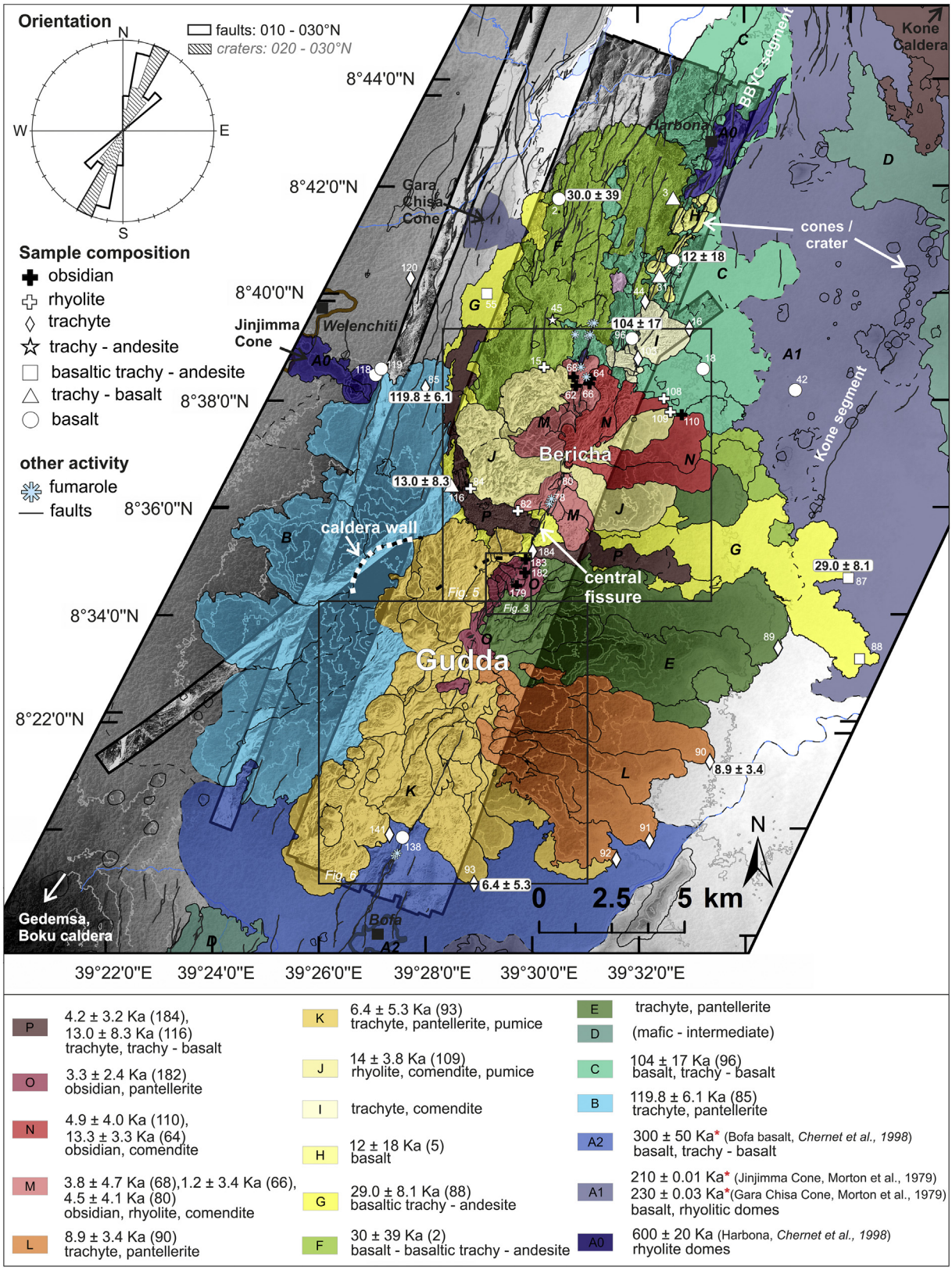

Fig. 4. Map of the BBVC. Different colours denote eruption phases from old to young (blue to red, as in Fig. 7) showing the temporal and spatial evolution of lava flow emplacement. Aerial LiDAR data were collected within three main strips over the volcanic edifice and indicate topography and morphology of lava flows and tectonic structures. Most recent activity is indicated by fumaroles along the main fissure system and the youngest eruption phases (N, P and O, red). The orientation of faults and alignment direction of crater and cones are shown in a length weighted rose diagram, and are consistent with the orientations measured from a more regional perspective by Muirhead et al. (2015). Composition of samples subject to bulk rock analysis are shown using symbols. Contour lines are in intervals of 20 m. Detailed maps of Bericha and Gudda are shown in Figs. 5 and 6.

and *Hillshade* for identification of lava flow edges cross-cutting relationships between volcanic and tectonic features (Figs. 3, 4).

3.4. Morphometric analyses

Morphometric analysis of lava flows enables an understanding of eruption activity, type and volume. This study utilised LiDAR and Aster remote sensing data to obtain length, thickness, area and volume for each eruptive phase. Length was measured by tracing the flow path from the source to the end of the flow (error ± 50–100 m). The thickness T is determined by measuring the difference in elevation of the lava flow edge and ground elevation. Volume of the eruption phases and the edifices of the BBVC were estimated by using a Generic Mapping Tools (GMT) volume calculation tool developed by Lara Kalkins described in Nomikou et al. (2014). This script calculates the difference between the surface morphology and an artificial smoothed surface for each exposed eruption phase polygon. For all individual lava flows and in particular for subhorizontal eruption phases volumes are estimated by the product of area and thickness assuming that thickness at the edge of the lava flow is representative of the entire lava flow.

3.5. Geochemical analyses

Petrographic observation and analyses of feldspar were performed with a polarising microscope and a Leo 1450VP scanning electron microscope (SEM) with an Oxford Instruments EDS detector at the University of Southampton. For whole rock analyses, 41 selected rock samples were crushed, soaked in water for 3–6 h and dried in 60 °C for 12 h. The samples were ground in agate to avoid contamination. For each sample, the Loss on Ignition (LOI) has been determined by weighing before and after 100 °C and 750 °C (felsic rocks) or 1000 °C (mafic rocks). Glass discs for analysing major elements were prepared with lithium tetraborate grains on the propane-oxygen gas Vulcan Fusion instrument. Whole rock analyses were undertaken with the Philips MagiX Pro Xray fluorescence spectrometer at the University of Southampton. Analytical precision and accuracy were monitored by standards.

3.6. Geochronology

An absolute timescale for the eruption history of the BBVC is provided by $^{40}Ar/^{39}Ar$ dating of 16 feldspar and groundmass separates of lava flows (Figs. 4–7, Table 1, A.1, A.2). Samples for $^{40}Ar/^{39}Ar$ dating were selected to achieve a representative geographic and compositional distribution (Fig. 4). Groundmass samples were screened for potassium content and degree of alteration. Feldspar separates were selected based on potassium content, low or negligible degree of alteration, crystal morphology (tendency towards euhedral shapes) and lack of inclusions. Sample preparation took place at the NERC Argon Isotope Facility (AIF) hosted by the Scottish Universities Environmental Research Centre (SUERC) in East Kilbride. Samples were pulverized in a jaw crusher, sieved and washed to obtain a 250–500 μm fraction and leached in 25% HNO_3 to remove altered phases. Feldspars were separated using magnetic Frantz machine and leached ultrasonically with 5% HF for 3–5 min (some required several runs) to remove adhering glass and groundmass, followed by repeated rinsing in distilled water and drying at T < 100 °C. Hand picking under a binocular microscope provided 1 g of clean and inclusion-free feldspar and groundmass separates for each sample.

4. Results

4.1. Geological map of the BBVC – relative and absolute chronology of lava flows

Based on the integration of high resolution DEM (LiDAR, Aster), satellite, aerial and Landsat images, field observations and geochemical data, the BBVC can be divided into four main eruptive stages: (1) rift floor basalts, (2) formation of Gudda Volcano in two main cycles ("old" Gudda and Gudda), between which caldera formation occurred, (3) the formation of Bericha Volcano, and, (4) sporadic fissure eruptions recurring between those stages. Stages (1) and (4), described together as rift floor activity, are most likely formed by fissure eruption, and are difficult to differentiate as individual eruption events.

These four broad stages are further differentiated into 16 eruption phases (A to P) (Figs. 4–6, 8, 9), defined as several discrete eruptions of the same style that are spatially and temporally clustered. In total, ~128 discrete lava flows (excluding rift floor) were identified and assigned to an individual eruption phase based on a combination of eruption type, composition, morphology, morphometry and degree of vegetation and weathering. A relative chronology of the eruption phases was determined primarily by cross-cutting relationships, in addition the above criteria. The relative chronology was combined with an absolute chronological framework provided by $^{40}Ar/^{39}Ar$ dating (Table 1, Fig. 7). We expect phases with many lava flows to have a greater age range. The synthesis of the eruption history of the BBVC is described in the following section based on the four main eruption stages, starting with the earliest.

4.1.1. Rift floor and fissure eruptions

Fissure eruptions occur episodically before and between the main eruptions of Gudda and Bericha, showing evidence for reactivation on several occasions, and are likely the source of the rift floor basalt (phase A1, A2), underlying the main BBVC. Fissures are characterized by tectonic fractures and chains of cones, craters and domes (phase A0, C, H), dominantly situated along the Boset-Kone segment (Fig. 4). Fissure lava flows with distinct sources are north and northeast of Bericha (phases F, C, I), whereas phases G and P are located between the Gudda and Bericha edifices (Figs. 4, 5, 8, 9).

4.1.1.1. Rift floor basalts (phase A1, A2 ~300 ka, D 104 ± 17 ka to 29.0 ± 8.1 ka). The oldest rocks exposed, phase A, occur as rift basalts, predate the main BBVC edifice and are exposed north (A1) and south (A2) of the BBVC (Figs. 4, 7-9), with the southern basalt belonging to the *Bofa Basalt Formation* (Kazmin et al., 1979; Brotzu et al., 1980, 1981; Chernet et al., 1998). Mapping of these rift floor basalts is challenging due to Quaternary cover, but the total thickness of both phases is estimated to be ~10 ± 5 m. The exposed northern part (phase A1 ~228 km^2) is assumed to be sourced from fissures of the Kone segment and is buried by flows of the Boset segment north of the BBVC, whereas a potential source for the mapped Bofa basalt (phase A2 ~98 km^2) is a covered fissure beneath or south of the BBVC. The Bofa Basalt is elevated ~100 m above the northern basalt, which can only be partly explained by the topographic trend of decreasing elevation towards Afar (Fig. 1). Lava flows from Gudda Volcano clearly post-date these rift floor basalts, most immediately by phase B (Fig. 4). After volcanism associated with Gudda had started, a further phase of rift floor basalt volcanism occurred (phase D ~153 km^2) to the north-east and south-west, likely sourced by reactivation of the Kone segment and Sodore lavas, respectively. The age range of phase D can be constrained by cross-cutting relations and morphology to 104 ± 17 ka to 29.0 ± 8.1 ka (Figs. 4, 8, 9).

4.1.1.2. Cones, domes and craters on the BBVC segment (phase A0, C 104 ± 17 ka, H 12 ± 18 ka). Cones and craters are aligned along fissures on the BBVC and Kone segment north of the BBVC edifice, whereas southwest of the BBVC there is less clear alignment along the tectonic fabric (Figs. 3, 4, 8, 9). Based on $^{40}Ar/^{39}Ar$ dating, at least two different phases, C (~45 km^2; 104 ± 17 ka, possible source for the basaltic lava flows C01–C03 (Fig. 5)) and H (~2.3 km^2; 12 ± 18 ka) along the cone chain on the BBVC segment north of the BBVC, can be identified, and suggest reactivation of this fissure on several occasions. Dome structures (phase A0, ~10 km^2), mapped on the northern BBVC segment and west of Bericha edifice, likely pre-date the basaltic rift floor.

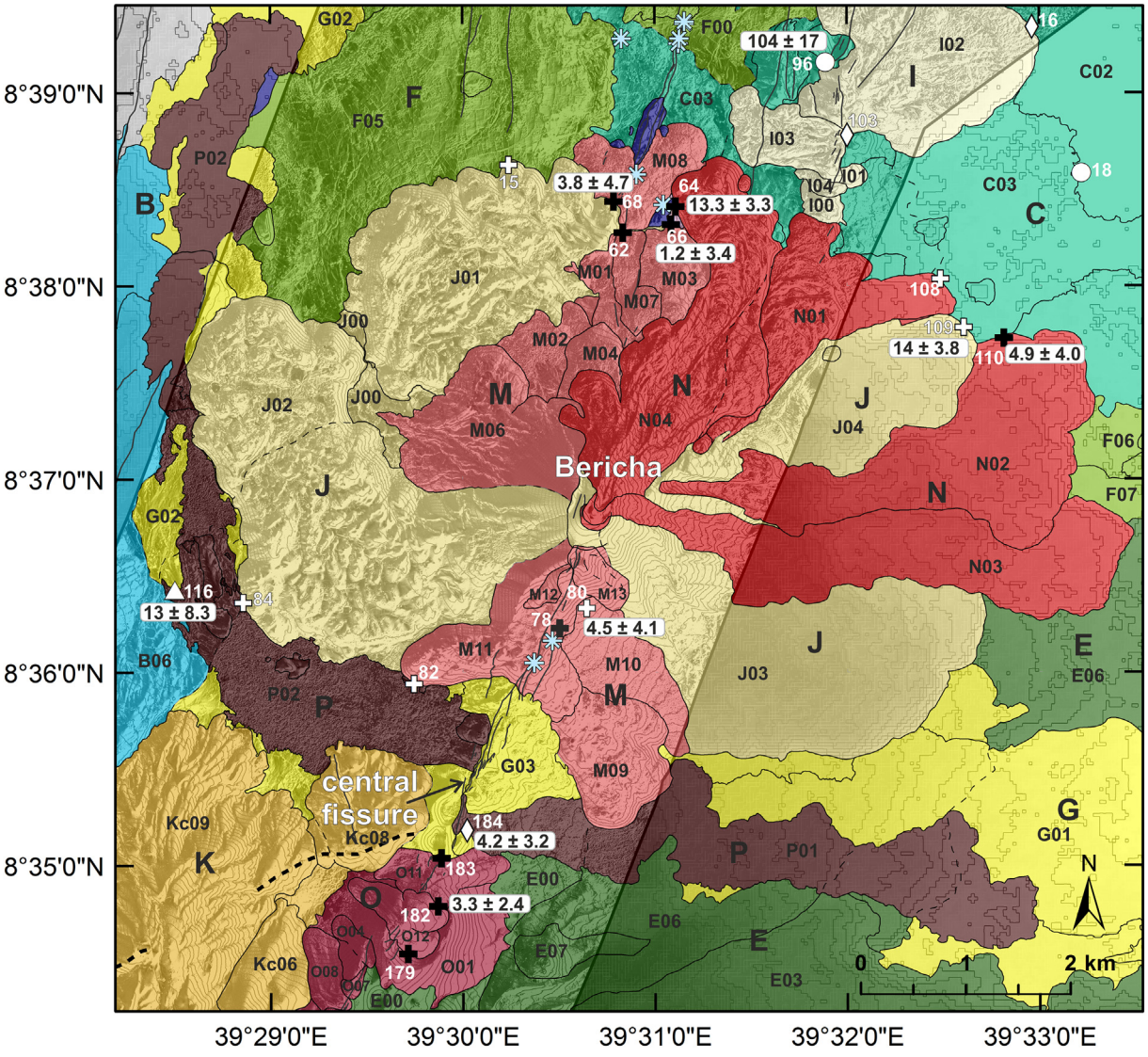

Fig. 5. Map of Bericha Volcano and fissure eruption between both volcanic centres of the BBVC with detailed lava flow chronology within eruptive phases. Colours and symbols are the same as on the map of the whole edifice of the BBVC (Fig. 4). $^{40}Ar/^{39}Ar$ ages in ka indicated with the white square and relative phase indicated by letter. Contour lines are in intervals of 20 m.

Morphology of cones, sources and topographic steps of the north eastern slope of Bericha Volcano and on Gudda (phase O, K, L) suggest a continuation of the cone chain of the BBVC segment below and near the summit of the BBVC (Figs. 4, 5, 8, 9).

4.1.1.3. Phase F (30 ± 39 ka). Fissure eruptions of phase F (36 km^2; at least six lava flows; flow F01 30 ± 39 ka) took place parallel to, but offset from, the main rift axis, and are most likely sourced from several truncated NNE-SSW fissures north of the BBVC or from the axial fissure pre-dating Bericha (Figs. 4, 7, 8, 9). This phase formed between the rift floor basalts (phase A, D) and Bericha (phase J). The eastern lava flows (F06–F07) pre-date phase M (Fig. 5). The dated flow is partly covered by the oldest lavas of phase G.

4.1.1.4. Phase I (>14 ± 3.8 ka). Phase I (4 km^2; five lava flows (I00–I04)) occurs to the north-east of Bericha (Figs. 4, 5, 8, 9), covering the rift axis (I00, I01, I04), as well as flowing towards the west (I03) and northeast (I02) from the fissure. These lava flows post-date the basalts and cinder cones of rift floor activity belonging to phase C (104 ± 17 ka) and predate phase J and phase N of Bericha Volcano. Thus, their age can be constrained to be between 104 ± 17 ka and 14 ± 3.8 ka.

4.1.1.5. Phase G (29 ± 8.1 ka) and P (13 ± 8.3 ka west, 4.2 ± 3.2 ka east). The largest exposed fissure eruptions occurred along the central NE-SW trending rift axis between Bericha and Gudda (Figs. 4, 5, 8, 9). This part of the rift axis was tectonically and magmatically reactivated on at least two occasions (phase G, P). The lavas flowed towards the southeast and northwest. During phase G (28 km^2; 3 mafic lava flows; flow G01 29 ± 8.1 ka) the oldest flow (G01) moved towards the southeast and was followed by alternating flows towards both sides of the fissure. Cross-cutting relations indicate that both phases (G and P) post-date the phase B and E on the eastern side and phase F phase on the western side. The older flows in phase G on both sides of the fissure (G00–G02) (Figs. 4, 5) appear to pre-date the first Bericha phase (J). In the last eruptive phase P (9 km^2; 2 lava flows; flow P02 west 13 ± 8.3 ka and flow P01 east 4.2 ± 3.2 ka) fissure lavas post-date Bericha's eruptive phases J and M and have characteristically dark (fresh) appearance in satellite images. Different compositions of lavas in phase P indicate individual eruptions even if absolute ages are within error.

4.1.2. Gudda Volcano

Lava flows can be subdivided into at least five different eruptive phases (B, E, K, L, O). Multiple eruption centres, including cones, craters,

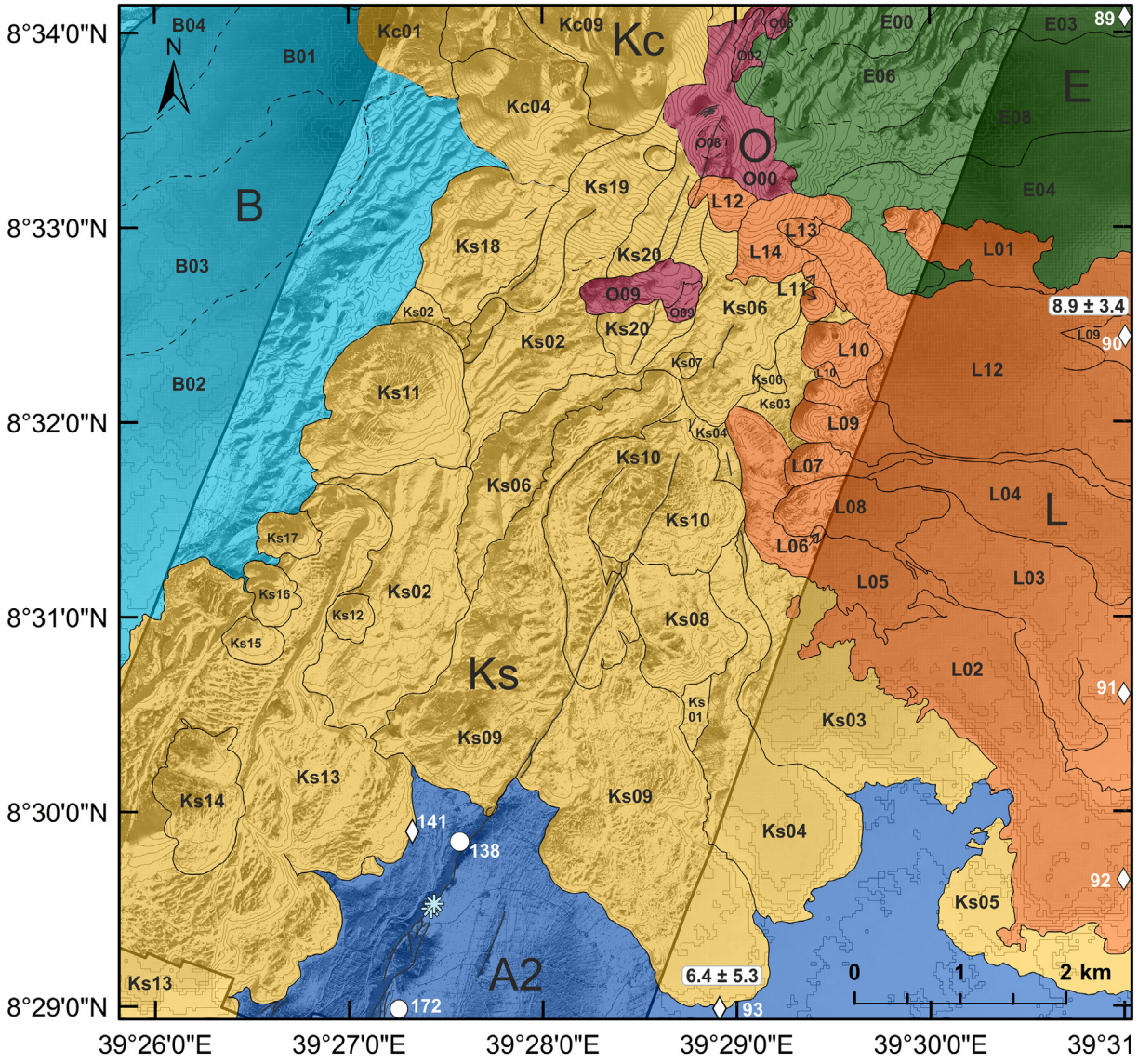

Fig. 6. Map of lava flows of post-caldera phases at Gudda Volcano with detailed lava flow chronology within eruptive phases. Colours and symbols are the same as on the map of the whole edifice of the BBVC (Fig. 4). $^{40}Ar/^{39}Ar$ ages in ka indicated with the white square and relative phase indicated by letter. Contour lines are in intervals of 20 m. Samples shown on the right-hand edge of the map were taken at the edge of the lava flow(off the map) in which the symbol is shown.

fissures and a remnant caldera are aligned along the main rift segment at the summit of Gudda (Figs. 3, 4). Based on distribution, flow direction and cross-cutting relations of lava flows, Gudda can be divided into pre-caldera activity on the western side (phase B) and post-caldera activity on the southern, central and eastern sides (phase E, K, L, O).

4.1.2.1. Phase B (119.8 ± 6.1 ka). Phase B (~71 km^2; at least 6 lava and pumice – lapilli deposits; B06 - 119.8 ± 6.1 ka) is mainly exposed on the western side of Gudda and represents a part of "old" Gudda edifice. It either pre-dates or formed during the youngest caldera-forming event, and constituent deposits appear to have been truncated by the remnant caldera rim to the west (Figs. 4, 6–9). Based on the flow direction of the post-caldera lava flows (phase K, O), the eastern part of the caldera rim is assumed to be on the central rift axis of Gudda Volcano, or slightly west of it, covered by phases K and O. This unit is strongly affected by erosion and reworking. Our analysis suggests that the original caldera diameter is ca. 4 km (Figs. 4, 8).

4.1.2.2. Phase E (119.8 ± 6.1 and 29.0 ± 8.1 ka). Phase E (~43 km^2) contains 9 thick lavas that flowed from the central rift segment on Gudda towards the east (Figs. 4, 6, 9). A possible extension of this unit could underlie lava flows of Bericha. The eruption age range is constrained to be between 119.8 ± 6.1 and 29.0 ± 8.1 ka, as it post-dates phase B and pre-dates a fissure eruption NE of it and lava flows of phases G, J and P.

4.1.2.3. Phase K (6.4 ± 5.3 ka). Phase K (55 km^2; 28 lava flows; flow Ks10 6.4 ± 5.3 ka) represents post-caldera activity and is mainly exposed on the southern side (Ks) and central part of Gudda Volcano (Kc) with lava flows sourced from multiple cones and craters along the rift axis (Figs. 4, 6–9). The central part pre-dates the fissure eruption of phase O and post-dates phase B, as it flowed from the rift axis down into the caldera and covers the eastern caldera rim and floor. Based on cross-cutting relations, the southern part of phase K post-dates (6.4 ± 5.3 ka) phase B and pre-dates lava flows of phase L and O. Lava flows of the central part of this phase (~13 km^2, 8 lava flows Kc1-Kc9) are significantly affected by erosion compared to the southern part (Ks) and lava flows of phase E. The southern part of phase K (~42 km^2, at least 21 different lava flows) has multiple sources along the main fracture system on the southern edifice slope.

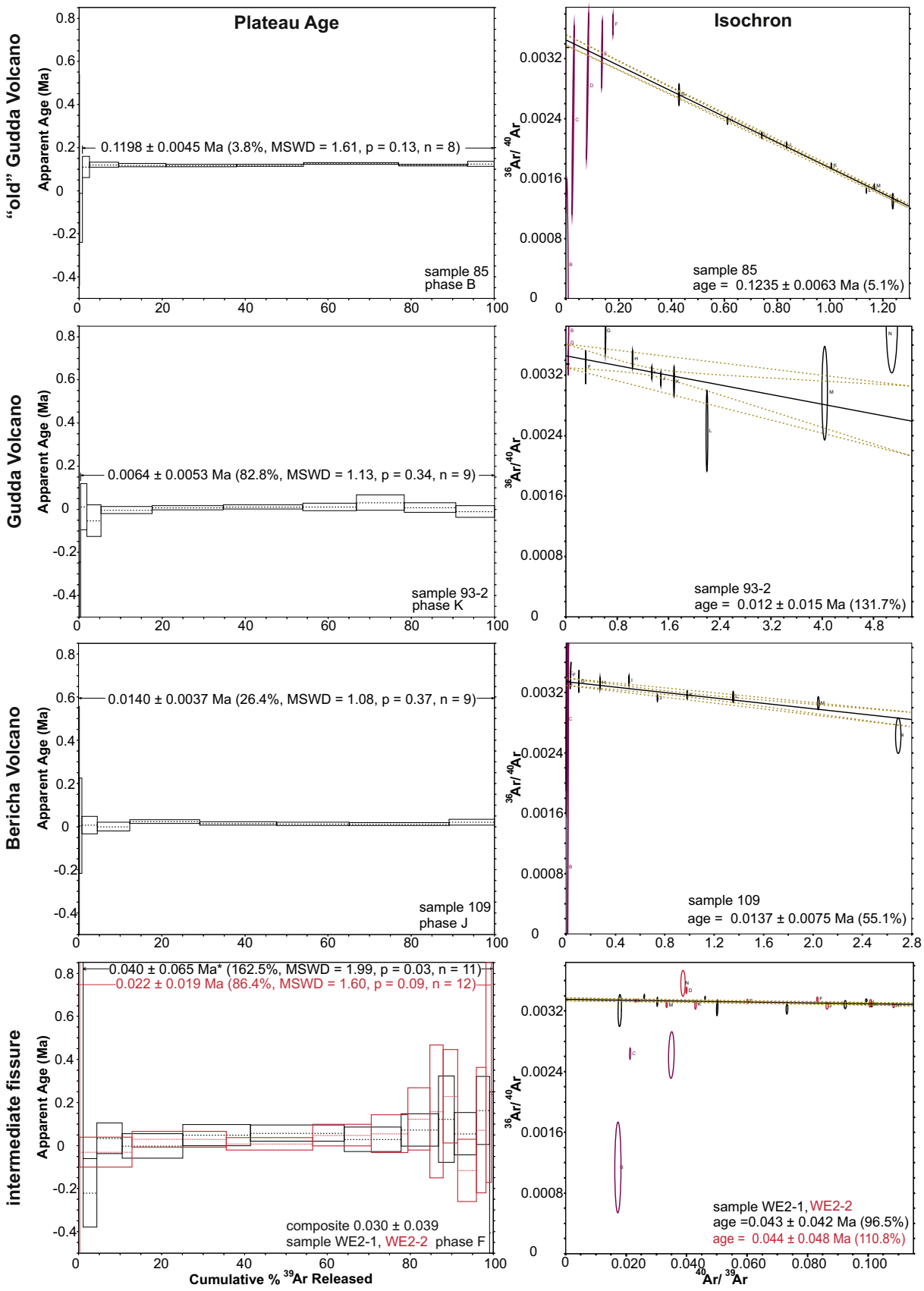

Fig. 7. Representative $^{40}Ar/^{39}Ar$ step-heating spectra plateau and isochron ages here shown for 4 samples from "old" Gudda, Gudda, Bericha Volcano and the fissure between both edifices as an example of high quality results. Error increase with decreasing age is due to the lower resolution for younger samples as well as the lower potassium content in mafic lavas, but all analysed samples give a representative age for their eruption phases.

Table 1
$^{40}Ar/^{39}Ar$ analyses of 16 lava flows of the BBVC.

ID	Rock, phase	m	Run	Plateau age									Isochron age						
				Age (ka)	±2σ w/J	MSWD	p	steps	n/n − n_{tot}	Ca/K	±2σ	%^{39}Ar release	Age (ka)	±2σ w/J	n	MSWD	p	$^{40}Ar/^{36}Ar_{(i)}$	±2σ
Rift floor/fissure																			
96	Basalt, C	FS	1	94.0	23.0	1.5	0.19	G-K	5/11	6.9	1.0	81.9	86.9	59.5	5	2.0	0.11	299.5	8.3
		FS	2	103.0	36.0	0.8	0.57	h-n	7/10	12.0	7.2	96.6	115.1	49.3	7	0.8	0.54	297.6	2.0
		FS	3	126.0	33.0	0.7	0.75	d-n	11/16	7.6	1.3	93.1	117.8	44.0	11	0.7	0.70	299.6	4.1
		FS	**c**	**104.0**	**17.0**	0.9	0.56	d-n	23/23	10.3	2.4	100.0	107.2	22.1	23	1.0	0.51	298.2	1.8
WE2	Basalt, F	GM	1	40.0	65.0	2.0	0.03	D-N	11/13	36	28	98.9	43.1	41.6	11	2.2	0.02	298.3	3.5
		GM	2	22.0	19.0	1.6	0.09	a-l	12/13	49	18	99.5	43.7	48.4	12	1.7	0.08	296.4	4.5
		GM	**c**	**30.0**	**39.0**	1.8	0.01	a-N	23/23	37	18	100.0	39.2	33.9	23	1.8	0.01	297.7	2.8
88	Trachyandesite, G	GM	1	32.0	12.0	1.9	0.07	F-M	8/12	7.2	5.7	94.1	32.1	26.7	8	2.2	0.04	298.5	2.4
		GM	2	27.0	11.0	1.1	0.33	D-K	8/10	1.8	0.1	88.5	37.2	38.1	8	1.3	0.27	297.4	4.3
		GM	**c**	**29.0**	**8.1**	1.4	0.12	F-K	16/16	6.6	3.4	100.0	31.1	17.8	16	1.5	0.09	298.3	1.7
5B	Basalt, H	GM	1	13.0	27.0	1.0	0.40	F-M	8/12	18.4	19.3	97.0	15.5	48.9	8	1.2	0.30	298.4	2.4
		GM	2	11.0	24.0	1.0	0.44	D-J	7/11	4.7	0.6	80.3	58.2	87.6	7	0.9	0.49	295.2	5.7
		GM	**c**	**12.0**	**18.0**	0.9	0.51	D-M	15/15	15.3	10.0	100.0	20.6	43.3	15	1.0	0.46	298.0	2.4
184	Trachybasalt, P	**FS**	**1**	**4.2**	**3.2**	1.2	0.31	H-N	7/9	0.316	0.031	98.7	5.2	12.9	7	1.4	0.22	297.2	17.6
116	Basalt, P	GM	1	16.0	25.0	1.5	0.12	C-N	12/12	9.1	3.5	100.0	34.0	41.4	12	1.5	0.12	297.7	1.6
		GM	2	25.0	16.0	1.1	0.36	D-N	11/12	8.9	4.2	99.9	13.6	32.0	11	1.2	0.32	299.6	2.7
		GM	3	7.0	10.0	1.1	0.34	b-l	11/12	10.4	3.6	97.9	0.2	16.8	11	1.1	0.33	299.1	1.0
		GM	**c**	**13.0**	**8.3**	1.3	0.12	b-M	34/34	9.0	2.0	100.0	10.4	13.4	34	1.3	0.11	298.7	0.7
Gudda																			
85	Trachyte, B	**FS**	**1**	**119.8**	**6.1**	1.6	0.13	G-N	8/14	0.010	0.018	99.1	123.5	6.3	8	1.5	0.16	289.8	11.1
90	Trachyte, K	GM	1	9.0	4.5	1.1	0.39	c-m	11/12	0.32	0.03	98.3	15.7	8.1	11	0.7	0.72	296.2	2.2
		FS	2	8.8	5.2	1.2	0.32	h-n	7/12	0.48	2.05	83.7	7.6	12.3	7	1.4	0.23	300.5	15.6
		GM, FS	**c**	**8.9**	**3.4**	1.0	0.41	c-n	18/18	0.32	0.09	100.0	11.8	4.3	18	0.9	0.54	297.1	1.9
93	Trachyte, L	**FS**	**1**	**6.4**	**5.3**	1.1	0.34	F-N	9/11	0.266	0.020	99.6	11.6	15.2	9	1.2	0.29	289.2	26.8
182	Obsidian, O	**FS**	**1**	**3.3**	**2.4**	0.9	0.51	E-M	9/10	0.035	0.054	93.4	2.7	5.3	9	1.0	0.41	301.2	23.7
Bericha																			
109	Rhyolite, J	**FS**	**1**	**14.0**	**3.8**	1.1	0.37	F-N	9/9	0.074	0.004	100.0	13.7	7.5	9	1.2	0.28	299.1	8.7
68	Obsidian, M	**FS**	**1**	**3.8**	**4.7**	0.9	0.55	E-N	10/0	0.103	0.001	100.0	5.6	12.5	10	1.0	0.46	297.5	7.3
66	Obsidian, M	**FS**	**1**	**1.2**	**3.4**	1.0	0.47	F-N	9/9	0.066	0.001	100.0	4.5	10.1	9	1.0	0.43	295.3	9.0
80	Rhyolite, M	**FS**	**1**	**4.5**	**4.1**	1.4	0.18	E-N	10/10	0.197	0.006	100.0	0.6	6.9	10	1.4	0.18	303.6	7.5
110	Obsidian, N	**FS**	**1**	**4.9**	**4.0**	1.5	0.15	F-N	9/9	0.102	0.005	100.0	−1.6	11.9	9	1.5	0.15	313.0	24.8
64	Obsidian, N	FS	1	14.0	4.2	0.9	0.50	I-N	6/9	0.079	0.001	93.1	18.9	8.1	6	0.7	0.56	290.4	12.2
		FS	2	12.3	5.3	1.1	0.34	F-N	8/8	0.112	0.014	100.0	6.5	11.6	8	0.9	0.47	313.7	21.6
		FS	**c**	**13.3**	**3.3**	1.0	0.49	I-N	14/14	0.101	0.012	100.0	13.0	6.0	14	1.0	0.41	299.1	10.7

Run **c**: composite of 2–3 runs; note that bold characters signify plateau ages from composite runs. Nucleogenic production ratios, isotopic constants, decay rates and plateau age criteria are described in Appendix A.1. Raw data for individual runs are listed in complete table in Appendix A.2.

4.1.2.4. Phase L (8.9 ± 3.4 ka). Phase L (33 km^2, 12 flows, L00–L13; flow L08 8.9 ± 3.4 ka) consists of a radial chain of ten exposed craters and cones on the south-eastern slope of Gudda (Figs. 4, 6–9). Three lava flows within this phase (L04, L11, L13) are sourced by the main rift segment on top of Gudda. The lava flows of this phase cover and obscure the lava flows of phase K and A2 in the south-eastern part, as well as phase E in the eastern part. Compared to the dated lava flow of phase K, the lava of phase L is within error of the absolute age but is clearly younger based on the relative chronology of eruption. These observations suggest that phase K (southern part) and L erupted temporally relatively close to each other and the possibility of broadly coeval activity cannot be excluded.

4.1.2.5. Phase O (3.3 ± 2.4 ka). The third and youngest phase of Gudda (~4 km^2, flow O12 3.3 ± 2.4 ka) was erupted from craters and pumice cones along the rift axis on the central edifice of Gudda, closer to the fissure lava flows of phases G and P (Figs. 3–5, 8, 9). The flows constitute obsidian lava and are relatively small in comparison to other obsidian flows from the BBVC. Some of them infill the crater, while others flow down the crater walls. These flows post-date phase K. The relation between this unit and the fissure lava of phase P is unclear as although juxtaposed they do not crosscut. Absolute dating shows similar ages to phase P and N. It is possible that obsidian lava flows on the summit of Gudda's rift axis, mapped here as phase K, may represent an earlier flow of phase O.

4.1.3. Bericha Volcano

Bericha is composed of at least 21 lava flows, that erupted during three main exposed phases (J, M, N) (Figs. 4, 5, 7–9). In comparison to Gudda, Bericha's lava flows are distributed radially from one main crater source on the top of the edifice and only a few side vents on the northern and north-eastern slope. Relative chronology is determined by cross-cutting relations of Bericha's lava flows with other eruptive phases on the south-eastern and south-western slope of the Bericha edifice.

4.1.3.1. Phase J (14.0 ± 3.8 ka). Bericha's first eruption phase J (~19 km^2; five thick rhyolitic lava flows; flow J04 14.0 ± 3.8 ka) occurred on the western (flows J00–J02) and eastern slopes (flows J03, J04) of Bericha. Phase J post-dates phase B and G, based on cross-cutting relations on the western side of the edifice; phases E and G based on cross-cutting relations on the eastern side of the edifice; and phases C, F and I based on cross-cutting relations on the northern side of the Bericha edifice. The upper relative age limit can only be determined by cross-cutting

Fig. 8. Chronology of eruption phases at the BBVC based on relative cross-cutting relations of lava flows and absolute $^{40}Ar/^{39}Ar$ ages measured within this study. Phase A is divided into A0 for rhyolitic domes, A1 for the northern rift floor basalt and A2 for the southern rift floor basalt, based on existing K/Ar ages (Chernet et al., 1998). Age ranges for phase D, E, I are constrained by relative chronology.

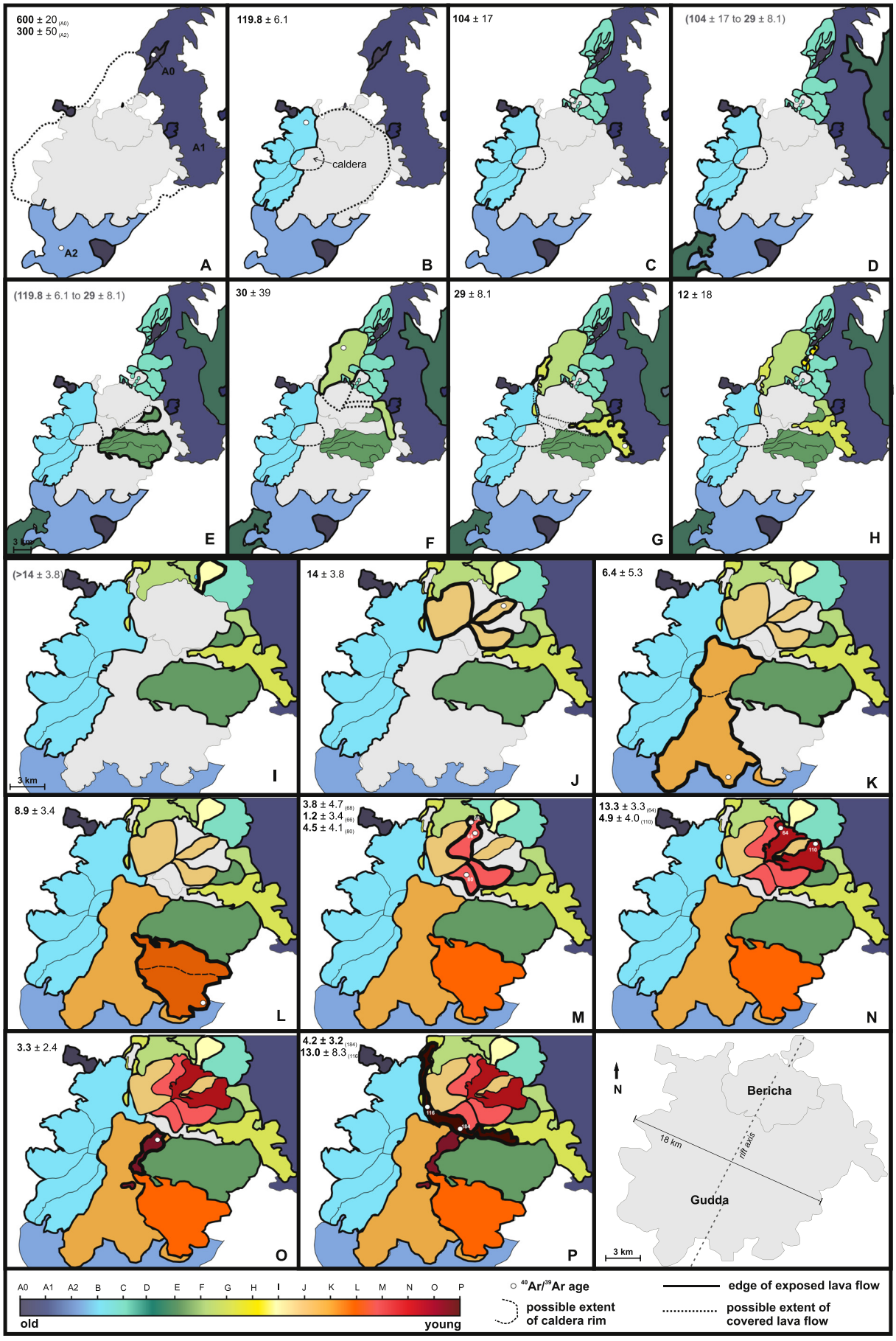
600 ± 20 (A0)
300 ± 50 (A2)
A0
A1
A2
A
119.8 ± 6.1
caldera
B
104 ± 17
C
(104 ± 17 to 29 ± 8.1)
D
(119.8 ± 6.1 to 29 ± 8.1)
3 km
E
30 ± 39
F
29 ± 8.1
G
12 ± 18
H
(>14 ± 3.8)
3 km
I
14 ± 3.8
J
6.4 ± 5.3
K
8.9 ± 3.4
L
3.8 ± 4.7 (68)
1.2 ± 3.4 (66)
4.5 ± 4.1 (80)
M
13.3 ± 3.3 (64)
4.9 ± 4.0 (110)
N
3.3 ± 2.4
O
4.2 ± 3.2 (184)
13.0 ± 8.3 (116)
P
N
Bericha
18 km
rift axis
Gudda
3 km
A0 A1 A2 B C D E F G H I J K L M N O P
old
young
40Ar/39Ar age
possible extent of caldera rim
edge of exposed lava flow
possible extent of covered lava flow

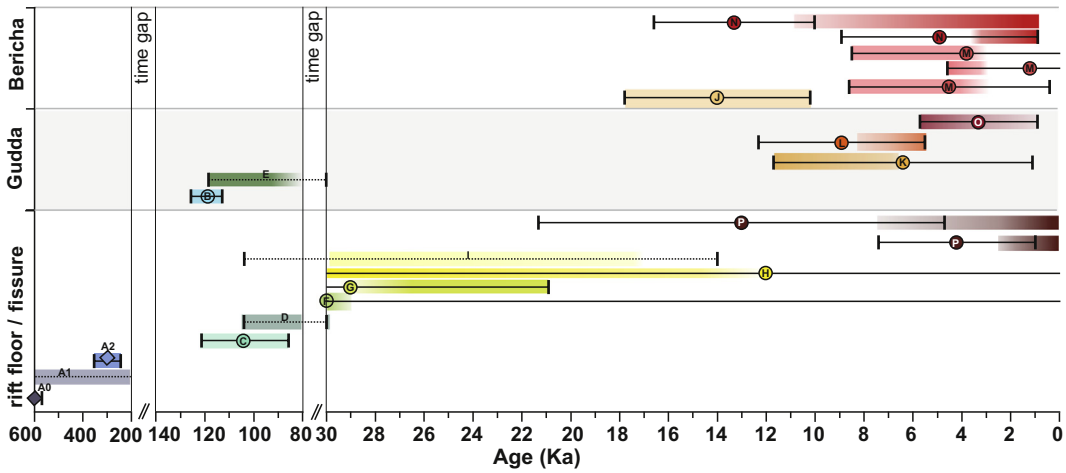

Fig. 9. Schematic diagram of magmatic activity at the BBVC classified into activity at fissures, Bericha Volcano, Gudda Volcano and on the rift floor. Error bars for absolute $^{40}Ar/^{39}Ar$ dating (solid) and constrained ages (dotted) are shown. Colours represent age likelihood based on absolute and relative chronology, with stronger colour indicating the most likely age range. Letters refer to eruption phases shown in Fig. 8.

relations with younger phases at Bericha (phases M & N). Thus, the age of phase J can be constrained to 29.0 ± 8.1 < phase J < 4.5 ± 4.1 ka, which is consistent with the $^{40}Ar/^{39}Ar$ age determination of flow J04 (Figs. 4, 5, 7–9).

4.1.3.2. Phase M. The second eruption phase M (8 km^2; 13 lava flows; flow M03 1.2 ± 3.4 ka, flow M08 3.8 ± 4.7 ka, flow M10 4.5 ± 4.1 ka) in the northern and southern part of Bericha was most likely sourced from different parts of the fissure on the rift axis running through the middle of Bericha (Figs. 4, 5, 8, 9). Cross-cutting relations demonstrate that the northern part clearly post-dates phase J and pre-dates phase N. The southern part may have erupted either during or after phase J, due to similar morphology and composition of at least two flows, or are broadly coeval to the northern part on the basis of similar absolute ages.

4.1.3.3. Phase N. Lava flows of the third eruptive phase N (~12 km^2; four lava flows; flow N02 4.9 ± 4.0 ka; flow N04 13.3 ± 3.3 ka) of Bericha overlay phase M and J, mainly in the north-eastern part of Bericha (Figs. 4, 5, 8, 9). The youngest lava flows (N03-N04) are sourced from the main crater, whereas lava flows N01 and N02 are sourced from side vents, aligned NE-SW and younging from lava flows of phase I towards the centre of Bericha. The youngest lava flow of Bericha (N04), determined by relative chronology and clear flow structures, flowed from the centre to north-north-east on top of lava flows (M03, M04, M07) of phase M.

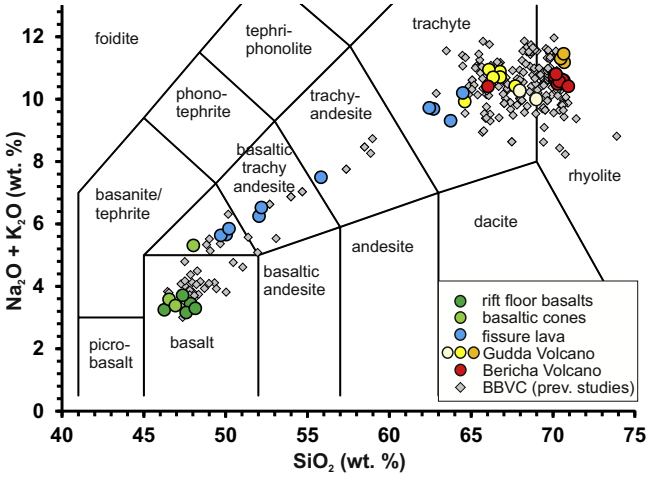

Fig. 10. Alkali verses SiO_2 diagram after Le Bas et al. (1986) shows a bimodal distribution from basalt towards trachyte (Gudda Volcano) and rhyolite (Bericha Volcano), which also includes one trachyte sample. Intermediate lavas are rare and mainly sourced by fissure eruption north and south of Bericha Volcano. Data from previous studies at the BBVC (grey diamonds) (Brotzu et al., 1974, 1980, 1981; Ronga et al., 2010; Macdonald et al., 2012) are consistent with this study.

4.2. Geochemistry of lava flows

4.2.1. Major element chemistry

Overall major element variation of the study area follows a basalt – trachyte – rhyolite pathway in terms of SiO_2 versus total alkali content (Le Bas et al., 1986) (Fig. 10). Specifically the BBVC has a bimodal composition ranging from basalt (rift floor basalts and scoria cones, phases A, C, D) to trachyte (Gudda phases E, K, L) and rhyolite (Gudda phase O; Bericha phases J, M, N) (Fig. 10, Table 2). Intermediate rocks are found in the associated fissure vents (phases F, G, I, P). The fissure northeast of Bericha (phase I) (Fig. 4) is most evolved with a trachyte composition (62.2 < SiO_2 > 64.4 wt%), and the fissure eruptions (phase F) are trachy-basaltic to basaltic trachy-andesitic (49.8 < SiO_2 > 55.9 wt%). The fissure between Gudda and Bericha is most variable with a

Table 2
Average whole rock compositions (wt%) and phenocryst assemblage (%) as examples for the main compositions.

	Rift floor	Fissure	Gudda		Bericha
	Basalt (n = 8)	Interm. (n = 9)	Trachyte (n = 7)	Rhyolite (n = 3)	Rhyolite (n = 12)
SiO_2	47.23	56.83	66.37	70.62	69.94
TiO_2	2.35	1.99	0.58	0.31	0.37
Al_2O_3	16.47	14.99	11.74	8.78	13.66
Fe_2O_3	12.35	9.74	8.71	8.37	4.25
MnO	0.18	0.24	0.35	0.30	0.18
MgO	6.23	2.42	0.07	−0.05	0.14
CaO	10.83	4.91	1.11	0.35	0.68
K_2O	0.64	2.43	3.98	4.33	4.66
Na_2O	2.99	5.37	6.47	6.98	5.90
P_2O_5	0.50	0.72	0.05	0.02	0.05
fs	20–25	2–15	20–35	10–15	5–25
ol	5–7	2–5	<5		<5
cpx	5–10	2–10	2–5	<5	<5
aenigm.			1–2	<1	
arfveds.			2–7	<5	
Opaque	<5	<5	1–2	1–2	<5
Vesicles	5–30	15–20		5–40	
GM	40–60, 95	50–85	60–95	70–95	65–90

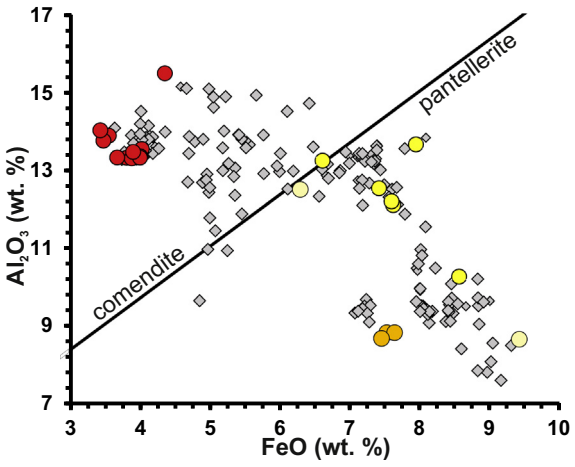

Fig. 11. Classification of peralkaline rocks after MacDonald (1974). Bericha has a comenditic composition and Gudda Volcano is mainly pantelleritic, whereas the samples of "old" Gudda Volcano has the highest FeO content. Symbols are explained in Fig. 10.

trachy-basaltic composition (phase P, west), basaltic trachy-andesite flow (phase G), and in places trachyte (phase P, east) (49.4 < SiO_2 > 63.7 wt%). Lavas from Gudda and Bericha are all peralkaline, defined by a molecular excess of Na_2O and K_2O over Al_2O_3 (i.e. peralkaline/agpaitic index) of 1.0–1.8 for Gudda, 1.0–1.1 for Bericha. Peralkaline lavas of Bericha are comendites (3.8–4.8 wt% FeO_{tot}, 13.2–15.5 wt% Al_2O_3), whereas Gudda's lavas have higher FeO_{tot} (7.3–10.5 wt%), Na_2O, MnO and TiO_2 and lower Al_2O_3 (8.8–13.6 wt%) and K_2O, and are pantellerites (Fig. 11). Typical compositions and a petrological summary of the BBVC lavas are shown in Table 2.

4.2.2. Whole rock chemistry over time

The compositional trends over time indicate bimodal (mafic – felsic) activity at the BBVC from 300 ka to present day with an apparent long term (regular) recurrent activity of mafic – intermediate lavas and a clustered distribution of felsic activity around 120 ka and in the last 16 ka (Figs. 9, 12). Intermediate fissure eruptions occur as a transitional phase before and during Gudda's and Bericha's felsic episodes in the last ~30 ka. The transitional phase shows a general trend from mafic towards felsic with increasing SiO_2 and alkali content and decreasing CaO and Fe_2O_3. Al_2O_3 shows a smooth decreasing trend over time. Lavas of Gudda differ most with lower Al_2O_3 and higher Fe_2O_3 contents (Fig. 12).

4.2.3. Feldspar analyses for $^{40}Ar/^{39}Ar$ dating

Feldspars are represented as plagioclases from bytownite to oligoclase up to anorthoclases, depending on whole-rock compositions. Basaltic rock samples contain plagioclase feldspars with a bytownite composition and an andesine to labradorite composition. Rhyolites contain feldspars, mainly anorthoclase and, subordinately, sanidine phenocrysts with a composition of $Ab_{70–79}$, $An_{0–2}$ and $Or_{20–29}$. Some phenocrysts exhibit a transitional composition from orthoclase to anorthoclase. Anorthoclase or sanidine bearing samples were targeted for $^{40}Ar/^{39}Ar$ dating as these phases are especially amenable to high precision dating. In contrast, holocrystalline groundmass fragments were used for dating basaltic rocks as these tended to be more potassic than associated plagioclase phenocrysts.

4.3. Morphometric analyses of lava flows

Morphometric analysis of lava flows was undertaken to characterize the type, size, geometry and volume of individual lava flows (Table 3) and for parent eruptive phases (Table 4, Fig. 13). Morphometric properties of individual lavas are presented in Table 4, differentiated by composition of mafic (phase A1, A2, C, D, H), intermediate (trachy-basalt to trachyte, phase F, G, I, P) and felsic (trachyte-rhyolite, phase B, E, J–O) lavas. Lava flow thickness increases with SiO_2 and alkali content from ~2 m (46 wt% SiO_2) to ~160 m (71 wt% SiO_2) (Table 3). Both mafic and felsic flows are characterized by a'a lavas. Felsic lava flows thicken at the flow front, whereas mafic flows thin at the edges. The thickest lava flows are rhyolitic flows of Bericha (phase J, ~160 m) and "old" Gudda deposits (phase B, ~120 m). Gudda's obsidian lava flows represent the thinnest felsic lava flows (phase O, 5–13 m). Composition, viscosity and cooling rate control the length of lava flows (Table 3), however for the more felsic lava flows of the BBVC, the flow size, topography and flow dynamics become more important factors. Areas for each eruption phase range between 3 and 71 km^2 for lava flow phases and between 45 and 228 km^2 for rift floor basaltic phases (Table 4). Fig. 13 illustrates a similar pattern of area and volume of each eruptive phase verses composition and time. The largest volume (3–5 km^3) and area (71–228 km^2) of eruptive phases are associated with the mafic northern rift floor basalts (phase A1, D), and the felsic exposed parts of "old" Gudda ~120 ka (phase B) and represent multiple events. Bericha's three eruption phases (J, M, N) together have a similar volume (4–5% of total volume) as one phase of Gudda. The Bericha edifice represents ~10% (volume and area) of the total BBVC edifice (Table 4).

5. Discussion

Our new absolute lava flow chronology, in conjunction with compositional and morphometric constraints, provide detailed new insights into the geological evolution of the BBVC, in particular the episodic distribution of eruptive activity over the past ~120 ka.

5.1. Compositional evolution

Since 120 ka, magmatism at the BBVC has been bimodal with recurrent mafic lavas and clustered felsic lava episodes (at 120 ka, and since 16 ka). We observe a general trend from dominantly mafic eruptions along a fissure system with minor felsic activity (from 100 to 30 ka), to dominantly felsic activity at Gudda and Bericha with sporadic fissure eruptions of intermediate compositions (from 30 ka to present) (Figs. 9, 12). This bimodal magmatism has been described in previous studies of the BBVC (Di Paola, 1972; Brotzu et al., 1974, 1980, 1981; Ronga et al., 2010; Macdonald et al., 2012), as well as at other Ethiopian rift volcanoes such as Gedemsa (Peccerillo et al., 2003), Fantale (Gibson, 1974) and others (Trua et al., 1999). Felsic compositions at the BBVC can be further subdivided into dominantly pantelleritic trachytes for post-caldera lavas at Gudda (phase E, K, L) and dominantly comenditic rhyolite for Bericha (phase J, M, N). These distinct differences support the presence of independent felsic magma reservoirs beneath Gudda and Bericha. Geochemical differences could be explained by additional feldspar crystallisation (e.g. Brotzu et al., 1980), due to low pressures in a shallow magma chamber, or by the presence of hydrous magmas at Gudda Volcano (e.g. Sisson and Grove, 1993; Blundy and Cashman, 2001).

Large volume eruptive phases (>1.0–0.5 km^3) generally constitute thick felsic flows of Gudda (phase B, E, K, L) and Bericha (phase J), but also include early rift floor basalts (phase A2, D), which cover large areas (Figs. 4, 13) and likely represent multiple eruptive events. The lavas included in this study have a total volume equating to ~25–30% (Table 4, excluding rift floor basalts) of the entire BBVC edifice, indicating a more extensive history of volcanism. Further, tephra layers around the BBVC, pumice cones (phase O) and the remnant caldera rim suggest that lava flow emplacement are associated with explosive eruptions. The prevalence of voluminous felsic lavas and absence of mafic lavas on Bericha and Gudda can be explained by the inability of mafic magmas to dynamically ascend through a relatively low-density felsic reservoir (i.e. a mafic 'shadow zone' (Walker, 1999)).

A major finding of our study is that the BBVC fissure system has been episodically active, with considerable geochemical variation along the

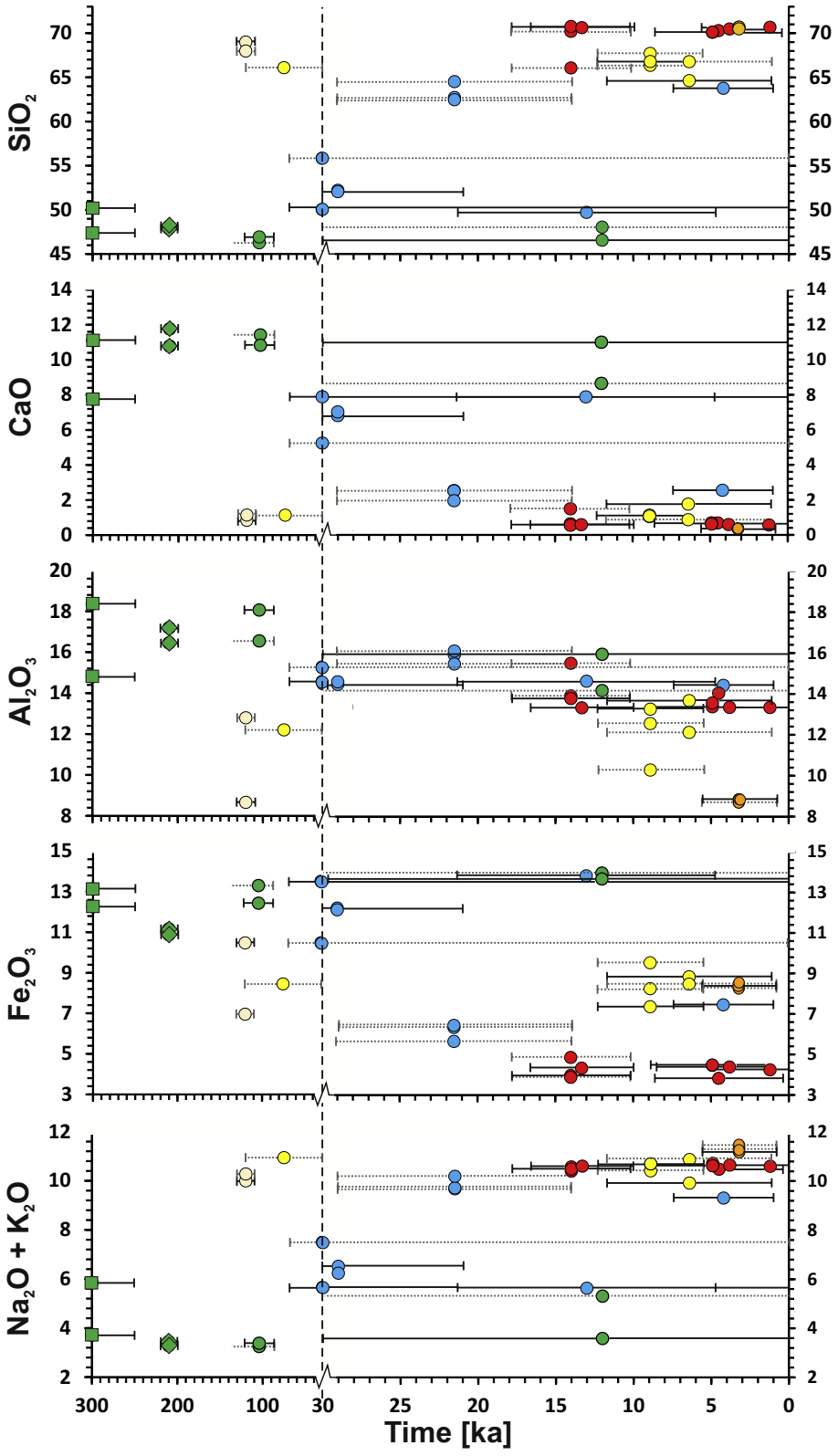

Fig. 12. Compositional evolution of the BBVC lava flows over time show a bimodal distribution with recurrent mafic activity and clustered felsic activity. Note the scale used on the x-axis changes at 30 ka. Colours indicate sample location and are the same as in Fig. 10. Error bars indicate error of absolute ages (black line) and relative range of non-dated lavas (grey dashed line) for BBVC lavas of this study (circle) and age constraints from Chernet et al. (1998) (square) and Morton et al. (1979) (diamond).

rift segment over time. The central fissure systems between both edifices (Figs. 4, 5) were reactivated on several occasions over the last 30 ka, with compositions changing from basaltic trachy-andesite (phase G) to trachy-basalt (phase P west) and trachyte (phase P east). The fissure system northeast of Bericha (Figs. 4, 5) changed in composition from basaltic (phase C, H) to trachytic (phase I) over the last

Table 3
Morphometric analyses of individual lava flows including thickness at the flow edge, length, area and volumes (based on estimated thickness and area measurements).

SiO_2 [wt%]	Thickness [m]		Length [km]		Area [km^2]		Volume [km^3]	
	Range	Average	Range	Average	Range	Average	Range	Average
Mafic (45–49)	3–36	15.8	0.7–6.9	2.81	0.26–225.64	6.74	0.003–4.357	0.57
Intermediate (49–65)	3–48	20.1	0.3–13.3	3.93	0.05–20.24	3.84	0.001–0.322	0.08
Felsic Gudda (65–71)	4–120	48.30	0.2–11.1	2.49	0.015–21.89	2.82	0.001–1.405	0.14
Felsic Bericha (69–71)	1.5–158	46.30	0.05–5.3	1.98	0.007–6.94	1.44	0.001–1.093	0.20

~104 ka. Further, fissure lavas belonging to phase I have a comenditic affinity, making these more likely to be a felsic outward fissure propagation from the Bericha plumbing system (Fig. 11). The composition of fissures north of Bericha (Fig. 4) varies from rhyolite (phase A0), to basalt (phase A1, C, H), trachy-basalt and trachy-andesite (phase F) with time (i.e. from 600 to 30 ka). A fissure eruption near the summit of Gudda changed composition from pantellerite trachyte to pantellerite rhyolite (phase O; Figs. 4, 5) within the last 10 ka, with geochemical trends consistent with fractional crystallisation (Figs. 10–12). On the whole, the observed spatio-temporal geochemical changes could be related to magmatic evolution, changing sources and/or growth of fracture systems tapping different magma storage levels or the upper mantle (Boccaletti et al., 1999). Further geochemical studies are ongoing to determine the contrasting pre-eruptive magmatic processes of Bericha and Gudda (Siegburg et al., in prep).

5.2. Episodic activity at the BBVC

The $^{40}Ar/^{39}Ar$ ages of lava flows reported in our study are generally consistent with the relative eruption chronology. In particular, absolute dated lava flows within the last felsic episode (since 16 ka), are mainly within error of each other (Fig. 9) and chronology is improved by observed field relationships. The only significant difference between our relative chronology and absolute $^{40}Ar/^{39}Ar$ ages are found in samples 116 (phase P) and sample 64 (phase N), where the absolute ages appear to be older than those interpreted from our relative chronology. Groundmass of sample 116 is dated in three runs (Table 1), but two of three runs are within error of the relative chronology. Although not apparent in the inverse isochron ages (Table 1; Appendix A.2), the third, older aliquot may be affected by subtle excess argon or xenocryst contamination. Feldspars in sample 64 show intergrowth textures and xenocrystic characteristics. We interpret the anomalously old apparent age for this sample as being affected by xenocrystic uptake immediately prior to eruption (e.g. Singer et al., 1998; Gardner et al., 2002).

Dated felsic and mafic activity around the BBVC occurred in two main episodes around ~1.6–1.4 Ma (Morbidelli et al., 1975; Chernet et al., 1998; Abebe et al., 2007) and <650 ka (Morton et al., 1979; Chernet et al., 1998). Additional mafic phases were very active during ~440–300 ka (Morton et al., 1979; Chernet et al., 1998) and ~104 ka, and formed extensive underlying rift floor basalts as well as basaltic cones. Later fissure eruptions at the BBVC are mafic to intermediate and likely represent reactivation of fissure phases with a ~10 ka frequency, recurring at ~30 ka (phases F, G), ~12 ka (phase H) and in the last ~6 ka (phase P) (Fig. 9). Further felsic activity at the BBVC occurred between the mafic episodes at ~840 ka, ~230–210 ka and between 160 ka (Morton et al., 1979) and ~119 ka ("old" Gudda). The last felsic episode is <16 ka (14 ka, 8 ka, <5 ka) (Fig. 9), and represents large volume post-caldera activity at Gudda Volcano and formation of Bericha Volcano. The 3 main felsic episodes over the last 230 ka (~230 ka, ~119 ka, since ~16 ka) might suggest an overall frequency of around ~100 ka, similar to that reported for Aluto volcano (Hutchison et al., 2016b). The temporal distribution of mafic and felsic magmatism around the BBVC suggests that this part of the magmatic segment experienced regular and recent felsic activity. Over the last ~30 ka, mafic to intermediate fissure activity potentially stimulated reactivation of felsic activity (over the last ~16 ka), manifested as peralkaline lava flows and explosive eruptions at Gudda and Bericha (Fig. 9); additional work is required to test this hypothesis. The overall dominance of felsic volcanism in the BBVC is likely due to the relatively early stage of rifting (stretching factor < 2), insofar as relatively thick continental crust encourages melt storage and fractional crystallisation. This contrasts with the more developed Afar rift, where dominantly basaltic volcanism is observed (e.g. Barberi and Varet, 1970).

An unexpected finding of this study is the young age of the latest large-volume felsic episode, since 16 ka. This magmatic episode represents the climax of peralkaline lava flow eruption for rhyolitic lavas of Bericha (phase M and N) and trachytic post-caldera activity at Gudda (phase K south, L, O), as well as fissure eruption between both edifices (phase P). Our finding that the last felsic episode at Gudda and Bericha (Fig. 9) are broadly coeval corroborates previous field observation (Brotzu et al., 1980). Average ages for dated lavas seems to be slightly older for Gudda compared to Bericha (Fig. 9, Table 1). The morphology and size of the edifice, as well as variation of eruption style and sources of Gudda and Bericha support the interpretation that Gudda is generally older with a more mature magmatic plumbing system. Given their proximity, Gudda and Bericha may interact hydraulically, or through stress transfer (e.g. Biggs et al., 2016), but compositionally they develop independently. Our chronology suggests that the most recent eruption of the BBVC was either a rhyolitic eruption sourced from Bericha (phase N), a mafic-intermediate fissure eruption between Gudda and Bericha (phase P), or a rhyolitic eruption of Gudda (phase O); further detailed tephrochronology is necessary to establish the relationships between these phases.

We now consider the recurrence rates of eruptions at Gudda and Bericha, focusing on well-exposed phases (Table 5). Stepwise mafic/

Table 4
Morphometric analyses summarised for each eruption phase. *Ages for phase A are K-Ar ages measured by Chernet et al. (1998), all other are $^{40}Ar/^{39}Ar$ ages from this study. For quoted values in text we used preferentially eruption phase volumes calculated by GMT and volume estimation for sub-horizontal eruption phases.

Phase	Age [ka]	Area [km^2]	Volume [km^3]			
		Exposed	Measured	Min	Max	GMT
A0	600* ± 20	9.67	0.695	0.427	0.777	0.588
A1	–	228.26	4.384	1.825	5.485	–
A2	300* ± 50	98.49	1.182	0.492	1.477	–
B	119.8 ± 6.1	71.21	4.987	3.468	8.645	–
C	104 ± 17	45.08	0.701	0.255	0.937	–
D	–	153.82	2.669	0.938	3.449	–
E	–	42.83	2.464	1.805	4.610	1.353
F	30 ± 39	36.28	0.950	0.589	1.362	–
G	29 ± 8.1	27.88	0.413	0.294	0.921	–
H	12 ± 18	2.27	0.135	0.042	0.145	0.044
I	–	3.91	0.136	0.113	0.248	0.103
J	14 ± 3.8	18.56	2.601	1.781	3.160	0.647
K central	–	12.84	0.931	0.752	1.075	1.520
K south	6.4 ± 5.3	42.18	3.428	2.117	4.779	1.353
L	8.9 ± 3.4	33.19	2.635	1.960	3.252	1.110
M	4.5 ± 4.1	8.42	0.468	0.332	0.565	0.173
N	3.8 ± 4.7	11.83	0.812	0.544	1.002	0.279
O	3.3 ± 2.4	3.93	0.377	0.207	0.420	0.083
P	4.2 ± 3.2	8.72	0.081	0.017	0.182	0.025
Gudda		195.58	45.636			40.8
Bericha		41.23	9.620			4.48
BBVC		279.36	65.183			53.7

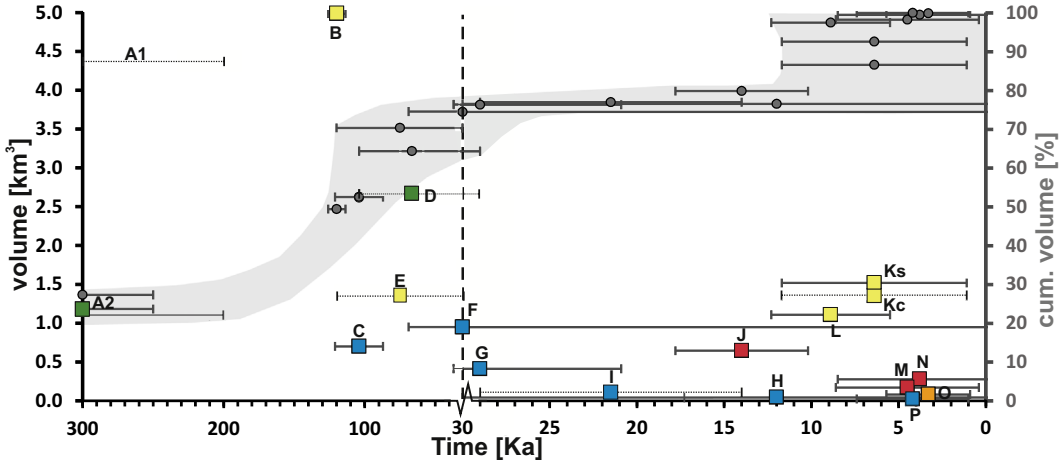

Fig. 13. Volume for each eruption phase (square) versus time with colour indicating composition (see Fig. 10). Rift floor basalts (phase A1, A2, D) and felsic activity at Gudda (phase B, E, K, L) are the most voluminous phases. Cumulative volumes (circle, grey shaded) show two main steps, coeval with felsic eruption episodes ~120 ka and since 16 ka. Note the change in time scale at 30 ka. Error bars indicated by only using relative chronology (dotted) and absolute $^{40}Ar/^{39}Ar$ ages (solid) of lava flows with the eruption phase.

intermediate dyke injection is associated with extension and magma assisted rifting within the MER, therefore the observed fissure eruptions at the BBVC are more frequent with an average eruption rate of <1/1000 years for the central fissure between Gudda and Bericha (phase G, P). Since major dyking episodes typically open an entire rift segment, as observed for the Krafla (e.g. Buck et al., 2006), Dabbahu (Wright et al., 2006) and Bardabunga (Sigmundsson et al., 2015) episodes, our interpreted rate is likely an under-estimate for the whole segment. Uncertainties for mafic phases are higher due to difficulties in differentiation of eruption events within mafic eruption phases (e.g. A, C, F, H). If we assume a dyke width of 0.5–2 m, and the current extension rate for the MER of ~ 5 mm/year (Bendick et al., 2006), we predict an average intrusion cycle of every 100 to 400 years for mafic dykes, equivalent to an average eruption rate of 2.5–10/1000 years.

For felsic eruptions, taking the entire post-caldera eruptive cycle since ~100 ka for Gudda (phase B excluded) and Bericha, the recurrence rate is <1/1000 years, broadly similar to other rift zones (Rowland et al., 2010). The latest felsic episode since ~16 ka includes 3 eruption phases of Bericha, and 3–4 at Gudda with much higher eruption rates and almost an order of magnitude higher productivity for Gudda compared to Bericha (Table 5). This episode formed the main part of the present-day exposed volcanic complex (Fig. 4). However, we stress that uncertainties are larger for Gudda, due to fewer absolute ages. The young age of lavas, evidence for regular episodic activity (Fig. 9, Table 1), and current fumarolic activity along the fault system (Fig. 4), suggest that the BBVC is still potentially active.

5.3. Comparison of timing of volcanic activity in the MER

1.6–0.1 Ma: A comparison between absolute ages of volcanic deposits at the BBVC and other central volcanoes in the MER shows that there is at least one large episode around 1.6 Ma and a further five episodes in the last 1 Ma, where activity of individual volcanoes of different rift segments were temporally clustered (Fig. 14). The oldest dated age at the BBVC edifice of around 1.6 ± 0.3 Ma (K/Ar) (Morbidelli et al., 1975) for ignimbrites southeast of the volcanic edifice and for volcanics of old Gudda (location unclear) suggest activity broadly coincident with many other silicic centres in the northern – central MER (Morton et al., 1979; Abebe et al., 2007). Basaltic activity of the rift floor southwest of the BBVC (i.e. close to Nazret), is K/Ar dated around 1.66 ± 0.03 Ma (Abebe et al., 2007) and around 1.44 ± 0.03 Ma (Chernet et al., 1998). Further periods of coincident activity of the BBVC and several rift segments in the last 1 Ma occurred at around 880–820 ka and 640–510 ka (Fig. 14), framing the dated activity at Gademotta caldera (Vogel et al., 2006). These activities are mainly around the older, eroded caldera structures for O'a caldera (Mohr et al., 1980), Boku (Morton et al., 1979) for both periods and Gedemsa (Morton et al., 1979) for the older period. Activity around the BBVC for this period is dated for volcanics (basalts and welded tuff) around Nazret southwest of the BBVC (Morton et al., 1979; Abebe et al., 2007) and for the rhyolitic dome (600 ± 20 ka) north of the BBVC (Chernet et al., 1998). Emplacement of the Bofa basalt (440 ± 50 ka (Morton et al., 1979) and 300 ± 50 ka (Chernet et al., 1998)), south of the BBVC, is temporally related to activity at Kone around 391 ka ± 10 ka (Vogel et al., 2006), Gedemsa caldera (Morton et al., 1979; Peccerillo et al., 2003) and O'a caldera (Mohr et al., 1980).

Significant overlap in timing of volcanism across the MER occurs between 320 and 140 ka (Fig. 14). This episode is characterized by magmatism and caldera collapse at Aluto Volcano around 316 ± 13 ka/306 ± 12 ka (Hutchison et al., 2016b) and Gedemsa 320–260 ka (Bigazzi et al., 1993; Peccerillo et al., 2003), followed by major ignimbrite eruptions and caldera collapses for O'a Shala 240 ± 30 ka (Mohr et al., 1980), Corbetti 182 ± 28 ka (Hutchison et al., 2016a, 2016b), Gademotta (Wendorf et al., 1975; Morgan and Renne, 2008), Fantale (Williams et al., 2004), mafic lava flows at Sodore (WoldeGabriel et al., 1990; Bigazzi et al., 1993), and formation of cones north of the BBVC at Jinjimma (210 ± 10 ka) and Gara Chisa (230 ± 30, 160 ± 10 ka) (Morton et al., 1979) (Fig. 4). For the BBVC edifice there is no absolute age for this 'flare up' episode dated in our study, possibly because "old" Gudda is mostly covered by younger flows. Activity around ~120 ka at "old" Gudda could be linked to be youngest part of the flare up activity episode (320–140 ka). Alternatively, it represents an individual felsic episode, broadly coincident with a 100 ka cycle for felsic activity at the BBVC (230–210 ka (Morton et al., 1979), ~120 ka and since ~16 ka). The 120 ka "old" Gudda deposits was formed at the same time as Bora Bericha Caldera (Bigazzi et al., 1993) (Figs. 1, 14),

Table 5
Eruption rate and production per 1000 years based on felsic magmatism at the BBVC in the last 16 ka and mafic – intermediate activity only along the central fissure between both edifices in the last 30 ka, calculated by number of flows/events and volume of phases.

	Time [ka]	Flows/events	Volume [km³]	Erupt. rate [per 1 ka]	Prod. rate [km³/1 ka]
Bericha	16	21	1	1–2	0.063
Gudda	16	50	9	2–5	0.563
Central fissure	30	4	0.5	<1	0.017

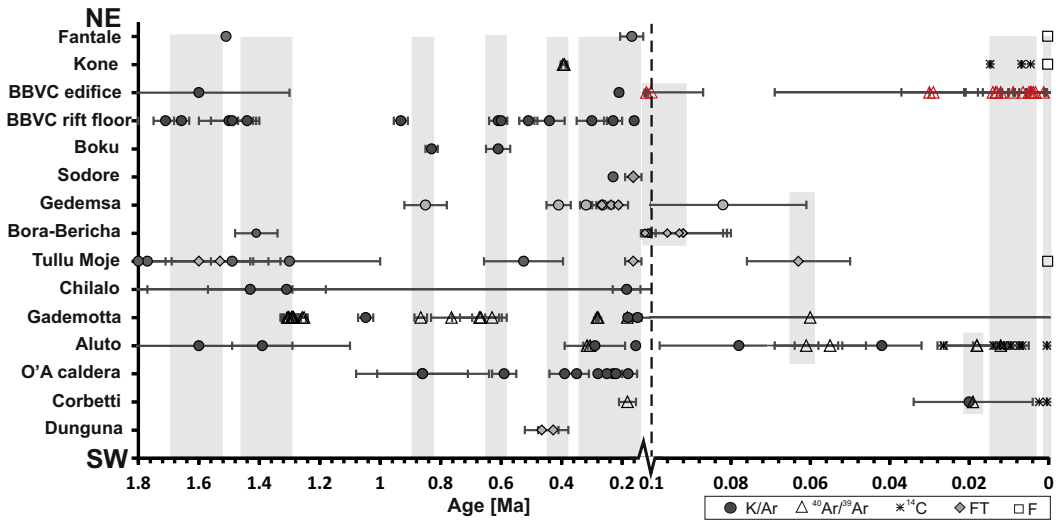

Fig. 14. Comparison of activity at the BBVC from this study (red) with other central volcanoes in the MER shown from southwest to northeast along the rift (Fig. 1), based on absolute ages and folklore (square). Dating method is indicated by symbol, K/Ar (grey circle), $^{40}Ar/^{39}Ar$ (triangle), ^{14}C (star), fission track (grey diamond). Note the change in the absolute age scale at 0.1 Ma (dashed line) to highlight our new ages alongside other Upper Pleistocene and Holocene volcanoes in the MER. References are provided within the text.

suggesting different rift segments were active at broadly the same time. The caldera collapse at the BBVC could feasibly have occurred in the 'flare up' episode, during formation of phase B (~120 ka), or later, but before eruption of the central part of Gudda (phase Kc) (Figs. 4, 6, 8). We stress that more detailed investigations of caldera deposits and "old" Gudda are necessary to test this further. Comparing the detailed eruption history of the BBVC (our study) and Aluto Volcano (Hutchison et al., 2016a, 2016b), both show evidence for ~100 ka cyclic large voluminous felsic activity, which might be applicable to other neighbouring volcanoes.

Since 100 ka, considerably fewer age constraints are available (Fig. 14), but this does not necessarily indicate a hiatus in activity. Notable clusters of activity are dated at ~60–55 ka at Aluto (Hutchison et al., 2016b), Gademotta (Vogel et al., 2006) and Tullu Moye (Bigazzi et al., 1993), and at ~20 ka at Aluto (Hutchison et al., 2016b) and Corbetti (Hutchison et al., 2016a, 2016b). The BBVC does not appear to have been active at these times, but relative chronology and errors of $^{40}Ar/^{39}Ar$ dates do not preclude the possibility of activity during this periods. Coincident activity at the BBVC (felsic and mafic), Kone (Williams et al., 2004) and Aluto (Hutchison et al., 2016a, 2016b) are around 14–10 ka. Coeval activity at Kone and the BBVC (Fig. 14) potentially suggests a rift segment-wide episode.

5.4. Possible processes for episodic activity

We observe episodic activity of clustered volcanic eruptions on 100 ka (felsic) and 10 ka (mafic) timescales at the BBVC, as well as on a range of spatial scales (e.g. within a single volcanic complex, rift segment, overall rift) in the MER. Episodic rifting has been observed in several rifts (e.g. Iceland, New Zealand, Afar, Atlantic) and explained by (a) a sudden release of tension, which affects the entire rift or is transferred between segments (e.g. Björnsson, 1985); (b) an acceleration in extension rate immediately prior to continental break up (Brune et al., 2016) resulting in higher melt production; (c) high mantle flux due to a change in melt fraction and viscosity (Gravley et al., 2016; Lamb et al., 2017); (d) pulsic mantle hotspot (Parnell-Turner et al., 2014) and e) magma evolution in the crust.

We favour the hypothesis that episodic mantle, crustal and tectonic processes interact to explain the observed trends of activity at the BBVC. Plate kinematic models do not suggest major changes in extension rate in the MER during the timescale of our study (e.g. Stamps et al., 2008). We interpret both episodic mantle flux, either from decompression melting caused by rifting (Gallacher et al., 2016) or the presence of a mantle hotspot (Schilling et al., 1992) to be plausible explanations. Both P- and S-wave tomographic imaging of the upper mantle show segmented low velocity anomalies beneath the MER and Afar (Hammond et al., 2013; Gallacher et al., 2016). The magnitude and segmented shape of the tomographic anomalies are interpreted as evidence for buoyancy driven decompression melting (Gallacher et al., 2016), which could cause temporal variations in melt flux. In addition, to date we have no evidence to rule out temporal changes in temperature or chemistry of hotspot flux over the timescale of our study. The observed differences in timing and cyclicity of mafic and felsic episodes can be explained by fundamental differences in magma formation and ascent. Mafic dyke emplacement is associated mainly with decompression melting, occurring broadly on the timescales of tectonic activity (Rooney et al., 2007). In contrast, felsic magma requires longer timescales to develop through fractional crystallisation and other crustal processes such as melting, storage, assimilation and homogenisation (Cashman et al., 2017), mainly during periods of tectonic quiescence (Boccaletti et al., 1999). Coeval activity within the BBVC and along the same magmatic segment may be caused by a hydraulic connection between different magma storage levels by sills and well-developed mush zones, whereas large volume eruptions, a shared deep magma source and broad extensional tectonic stress could affect several segments (Biggs et al., 2016).

6. Conclusions

The first detailed geological evolution of the Boset-Bericha Volcanic Complex (BBVC) is synthesised from field observations, morphometric analysis using high-resolution LiDAR data, geochemistry and new $^{40}Ar/^{39}Ar$ geochronology. This paper focused on understanding the eruption history of extensive young lava flows covering the two edifices, Gudda and Bericha. These lavas exhibit a bimodal composition ranging dominantly from basaltic rift floor lavas and scoria cones, to pantelleritic trachytes and rhyolite flows at Gudda, and comenditic rhyolites at Bericha. Intermediate compositions are associated with fissure vents along the Boset-Kone segment that link the silicic centres. Our analysis indicates that the BBVC can be described by four main eruptive stages:

1. early rift floor emplacement, (≥300 ka)
2. formation of Gudda Volcano within two main cycles, (~120 ka, since ~16 ka), separated by a period of caldera formation

3. formation of the Bericha Volcano (14 ka, since ~5 ka)
4. sporadic fissure eruptions (including episodes at ~104 ka, and since 30 ka).

Our new $^{40}Ar/^{39}Ar$ geochronology provides compelling evidence for episodic activity at the BBVC from ~120 ka to the present-day. Low-volume mafic episodes are more frequent (~10 ka cyclicity) than higher volume felsic episodes (~100 ka cyclicity). The most recent felsic episode occurred during the last ~16 ka. Felsic episodes have on average a higher eruption rate (2–5/1000 years) and productivity at Gudda compared to Bericha (1–2/1000 years). The voluminous lava eruptions from the BBVC at ~120 ka and since ~16 ka are coincident with dated activity at nearby volcanic centres in the MER.

Acknowledgments

We would like to thank the NERC Airborne Research and Survey Facility (grant ET12-14) for undertaking a LiDAR survey over the BBVC. We thank staff of the Institute of Geophysics, Space Science and Astronomy and Department of Earth Science at Addis Ababa University, Ethiopia for support during data collection (2012) and field work (2015). We thank R. Dymock and J. Imlach of the AIF laboratory at SUERC, and E. Roberts from University of Southampton for their assistance with sample preparation and $^{40}Ar/^{39}Ar$ measurement. We acknowledge the NERC Isotope Geosciences Facilities Steering Committee for funding to undertake $^{40}Ar/^{39}Ar$ dating at the Argon Isotope Facility (grant IP-1569-1115). We thank W. Hutchison and F. Illsley-Kemp for their helpful assistance with the GMT script for lava volume measurement. DK is supported by NERC grant NE/L013932.

Appendix A. Supplementary data

Supplementary data to this article can be found online at https://doi.org/10.1016/j.jvolgeores.2017.12.014.

References

Abebe, T., Manetti, P., Bonini, M., Corti, G., Innocenti, F., Mazzarini, F., Peckzay, Z., 2005. Geological map (scale 1:200,000) of the northern Main Ethiopian Rift and its implications for the volcano-tectonic evolution of the rift. Geol. Soc. Am. Map Chart Ser. MCH094 :pp. 1–20. https://doi.org/10.1130/2005MCH094TXT.

Abebe, B., Acocella, V., Korme, T., Ayalew, D., 2007. Quaternary faulting and volcanism in the Main Ethiopian Rift. J. Afr. Earth Sci. 48:115–124. https://doi.org/10.1016/j.jafrearsci.2006.10.005.

Aspinall, W., Auker, M., Hincks, T., Mahony, S., Nadim, F., Pooley, J., Sparks, S., Syre, E., 2011. Global Facility for Disaster Reduction and Recovery (GFDRR), volcano risk study. Volcano Hazard Expo. GFDRR Prior. Ctries. Risk Mitig. Meas., pp. 1–41

Barberi, F., Varet, J., 1970. The Erta Ale volcanic range (Danakil depression, northern Afar, Ethiopia). Bull. Volcanol. 34:848–917. https://doi.org/10.1007/BF02596805.

Bastow, I.D., Stuart, G.W., Kendall, J.M., Ebinger, C.J., 2005. Upper-mantle seismic structure in a region of incipient continental breakup: Northern Ethiopian rift. Geophys. J. Int. 162:479–493. https://doi.org/10.1111/j.1365-246X.2005.02666.x.

Bendick, R., McClusky, S., Bilham, R., Asfaw, L., Klemperer, S., 2006. Distributed Nubia-Somalia relative motion and dike intrusion in the Main Ethiopian Rift. Geophys. J. Int. 165:303–310. https://doi.org/10.1111/j.1365-246X.2006.02904.x.

Beutel, E., van Wijk, J., Ebinger, C., Keir, D., Agostini, A., 2010. Formation and stability of magmatic segments in the Main Ethiopian and Afar rifts. Earth Planet. Sci. Lett. 293:225–235. https://doi.org/10.1016/j.epsl.2010.02.006.

Bigazzi, B., Bonadonna, F.P., Di Paola, G.M., Giuliani, A., 1993. K-Ar and fission track ages of the last volcano tectonic phases in the Ethiopian rift valley (Tullu Moye area). Geol. Miner. Recources Somalia Surround. Reg. 113, pp. 311–322.

Biggs, J., Robertson, E., Cashman, K., 2016. The lateral extent of volcanic interactions during unrest and eruption. Nat. Geosci. 9:1–5. https://doi.org/10.1038/ngeo2658.

Bilham, R., Bendick, R., Larson, K., Mohr, P., Braun, J., Tesfaye, S., Asfaw, L., 1999. Secular and tidal strain across the Main Ethiopian Rift. Geophys. Res. Lett. 26:2789. https://doi.org/10.1029/1998GL005315.

Björnsson, A., 1985. Dynamics of crustal rifting in NE Iceland. J. Geophys. Res. 90:10151–10162. https://doi.org/10.1029/JB090iB12p10151.

Blundy, J., Cashman, K., 2001. Ascent-driven crystallisation of dacite magmas at Mount St Helens, 1980–1986. Contrib. Mineral. Petrol. 140:631–650. https://doi.org/10.1007/s004100000219.

Boccaletti, M., Mazzuoli, R., Bonini, M., Trua, T., Abebe, B., 1999. Plio-Quaternary volcanotectonic activity in the northern sector of the Main Ethiopian Rift: relationships with oblique rifting. J. Afr. Earth Sci. 29:679–698. https://doi.org/10.1016/S0899-5362(99)00124-4.

Brotzu, P., Morbidelli, L., Piccirillo, E.M., Traversa, G., 1974. Petrological features of Boseti Mountains, a complex volcanic system in the axial portion of the Main Ethiopian rift. Bull. Volcanol. 38:206–234. https://doi.org/10.1007/BF02597811.

Brotzu, P., Morbidelli, L., Piccirillo, E.M., Traversa, G., 1980. Volcanological and magmatological evidence of the Boseti Volcanic Complex (Main Ethiopian Rift). Atti Convegni Lincei 47, 317–366.

Brotzu, P., Ganzerli-Valenini, M.T., Morbidelli, L., Piccirillo, E.M., Stella, R., Traversa, G., 1981. Basaltic volcanism in the northern sector of the main Ethiopian Rift. J. Volcanol. Geotherm. Res. 10, 365–382.

Brune, S., Williams, S.E., Butterworth, N.P., Müller, R.D., 2016. Abrupt plate accelerations shape rifted continental margins. Nature 536:201–204. https://doi.org/10.1038/nature18319.

Buck, W.R., Einarsson, P., Brandsdóttir, B., 2006. Tectonic stress and magma chamber size as controls on dike propagation: constraints from the 1975–1984 Krafla rifting episode. J. Geophys. Res. Solid Earth 111:1–15. https://doi.org/10.1029/2005JB003879.

Calais, E., Ebinger, C., Hartnady, C., Nocquet, J.M., 2006. Kinematics of the East African Rift from GPS and earthquake slip vector data. In: Yirgu, G., Ebinger, C.J., Maguire, P.K.H. (Eds.), The Afar Volcanic Province Within the East African Rift System. Geological Society, London, Special Publications, London, pp. 9–22.

Casey, M., Ebinger, C., Keir, D., Gloaguen, R., Mohamed, F., 2006. Strain accommodation in transitional rifts: extension by magma intrusion and faulting in Ethiopian rift magmatic segments. Geol. Soc. Lond. Spec. Publ. 259:143–163. https://doi.org/10.1144/GSL.SP.2006.259.01.13.

Cashman, K.V., Sparks, R.S.J., Blundy, J.D., 2017. Vertically extensive and unstable magmatic systems: a unified view of igneous processes. Science (80-.) 355 (6331), eaag3055. https://doi.org/10.1126/science.aag3055.

Chernet, T., Hart, W.K., Aronson, J.L., Walter, R.C., 1998. New age constraints on the timing of volcanism and tectonism in the northern Main Ethiopian Rift - southern Afar transition zone (Ethiopia). J. Volcanol. Geotherm. Res. 80:267–280. https://doi.org/10.1016/S0377-0273(97)00035-8.

Cole, J.W., 1969. The Gariboldi volcanic complex. Bull. Volcanol. 33:566–578. https://doi.org/10.1007/BF02596525.

Cornwell, D.G., Mackenzie, G.D., England, R.W., Maguire, P.K.H., Asfaw, L., Oluma, B., 2006. Northern Main Ethiopian Rift crustal structure from new high-precision gravity data. In: Yirgu, G., Ebinger, C., Maguire, P.K.H. (Eds.), The Afar Volcanic Province Within the East African Rift System. Geological Society, London (pp. 259, 307–321).

Corti, G., 2009. Continental rift evolution: from rift initiation to incipient break-up in the Main Ethiopian Rift, East Africa. Earth Sci. Rev. 96:1–53. https://doi.org/10.1016/j.earscirev.2009.06.005.

Coulié, E., Quidelleur, X., Courtillot, V., Lefèvre, J.C., Chiesa, S., 2003. Comparative K-Ar and Ar/Ar dating of Ethiopian and Yemenite Oligocene volcanism: implications for timing and duration of the Ethiopian traps. Earth Planet. Sci. Lett. 206:477–492. https://doi.org/10.1016/S0012-821X(02)01089-0.

Di Paola, G.M., 1972. The Ethiopian Rift Valley (between 7° 00′ and 8° 40′ lat. North). Bull. Volcanol. 36:517–560. https://doi.org/10.1007/BF02599823.

Ebinger, C.J., Casey, M., 2001. Continental breakup in magmatic provinces: an Ethiopian example. Geology 29:527–530. https://doi.org/10.1130/0091-7613(2001)029<0527:CBIMPA>2.0.CO;2.

Fernandes, R.M.S., Ambrosius, B.A.C., Noomen, R., Bastos, L., Combrinck, L., Miranda, J.M., Spakman, W., 2004. Angular velocities of Nubia and Somalia from continuous GPS data: implications on present-day relative kinematics. Earth Planet. Sci. Lett. 222:197–208. https://doi.org/10.1016/j.epsl.2004.02.008.

Gallacher, R.J., Keir, D., Harmon, N., Stuart, G., Leroy, S., Hammond, J.O.S., Kendall, J.-M., Ayele, A., Goitom, B., Ogubazghi, G., Ahmed, A., 2016. The initiation of segmented buoyancy-driven melting during continental breakup. Nat. Commun. 7:13110. https://doi.org/10.1038/ncomms13110.

Gardner, J.E., Layer, P.W., Rutherford, M.J., 2002. Phenocrysts versus xenocrysts in the youngest Toba Tuff: implications for the petrogenesis of 2800 km^3 of magma. Geology 30:347–350. https://doi.org/10.1130/0091-7613(2002)030<0347:PVXITY>2.0.CO;2.

Gibson, I.L., 1974. Quaternary silicic volcanic centres in the Main Ethiopian Rift. Bull. Volcanol. 38, 791–802.

Gravley, D.M., Deering, C.D., Leonard, G.S., Rowland, J.V., 2016. Ignimbrite flare-ups and their drivers: a New Zealand perspective. Earth Sci. Rev. 162:65–82. https://doi.org/10.1016/j.earscirev.2016.09.007.

Hammond, J.O.S., Kendall, J.M., Stuart, G.W., Ebinger, C.J., Bastow, I.D., Keir, D., Ayele, A., Belachew, M., Goitom, B., Ogubazghi, G., Wright, T.J., 2013. Mantle upwelling and initiation of rift segmentation beneath the Afar Depression. Geology 41:635–638. https://doi.org/10.1130/G33925.1.

Harris, W.C., 1844. The Highlands of Ethiopia. vol. III. Longmans, London.

Hayward, N.J., Ebinger, C.J., 1996. Variations in the along-axis segmentation of the Afar Rift system. Tectonics 15:244. https://doi.org/10.1029/95TC02292.

Hofmann, C., Courtillot, V., Féraud, G., Rochette, P., Yirgu, G., Ketefo, E., Pik, R., 1997. Timing of the Ethiopian flood basalt event and implications for plume birth and global change. Nature 389:838–841. https://doi.org/10.1038/39853.

Hutchison, W., Fusillo, R., Pyle, D.M., Mather, T.A., Blundy, J.D., Biggs, J., Yirgu, G., Cohen, B.E., Brooker, R.A., Barfod, D.N., Calvert, A.T., 2016a. A pulse of mid-Pleistocene rift volcanism in Ethiopia at the dawn of modern humans. Nat. Commun. 7:13192. https://doi.org/10.1038/ncomms13192.

Hutchison, W., Pyle, D.M., Mather, T.A., Yirgu, G., Biggs, J., Cohen, B.E., Barfod, D.N., Lewi, E., 2016b. The eruptive history and magmatic evolution of Aluto volcano: new insights

into silicic peralkaline volcanism in the Ethiopian rift. J. Volcanol. Geotherm. Res. 328: 9–33. https://doi.org/10.1016/j.jvolgeores.2016.09.010.
Kazmin, V., Seife, M.B., Nicoletti, M., Petrucciani, C., 1979. Evolution of the Northern Part of Ethiopian Rift - Geodynamic Evolution of the Afro-Arabain Rift System. Accad. Naz. Lincei, Roma.
Keir, D., Kendall, J.M., Ebinger, C.J., Stuart, G.W., 2005. Variations in late syn-rift melt alignment inferred from shear-wave splitting in crustal earthquakes beneath the Ethiopian rift. Geophys. Res. Lett. 32:1–4. https://doi.org/10.1029/2005GL024150.
Keir, D., Ebinger, C.J., Stuart, G.W., Daly, E., Ayele, A., 2006. Strain accommodation by magmatism and faulting as rifting proceeds to breakup: seismicity of the northern Ethiopian rift. J. Geophys. Res. Solid Earth 111:1–17. https://doi.org/10.1029/2005JB003748.
Kendall, J.M., Stuart, G.W., Ebinger, C.J., Bastow, I.D., Keir, D., 2005. Magma-assisted rifting in Ethiopia. Nature 433:146–148. https://doi.org/10.1038/nature03161.
Keranen, K., Klemperer, S.L., 2008. Discontinuous and diachronous evolution of the Main Ethiopian Rift: implications for development of continental rifts. Earth Planet. Sci. Lett. 265:96–111. https://doi.org/10.1016/j.epsl.2007.09.038.
Lamb, S., Moore, J.D.P., Smith, E., Stern, T., 2017. Episodic kinematics in continental rifts modulated by changes in mantle melt fraction. Nature 547:84–88. https://doi.org/10.1038/nature22962.
Le Bas, M.J., Le Maitre, R.W., Streckeisen, A., Zanettin, B., 1986. A chemical classification of volcanic rocks based on the total alkali silica diagram. J. Petrol. 27:745–750. https://doi.org/10.1093/petrology/27.3.745.
MacDonald, R., 1974. Nomenclature and petrochemistry of the peralkaline oversaturated extrusive rocks. Bull. Volcanol. 38:498–516. https://doi.org/10.1007/BF02596896.
Macdonald, R., Bagiński, B., Ronga, F., Dzierzanowski, P., Lustrino, M., Marzoli, A., Melluso, L., 2012. Evidence for extreme fractionation of peralkaline silicic magmas, the Boseti volcanic complex, Main Ethiopian Rift. Mineral. Petrol. 104:163–175. https://doi.org/10.1007/s00710-011-0184-4.
Mackenzie, G.D., Thybo, H., Maguire, P.K.H., 2005. Crustal velocity structure across the Main Ethiopian Rift: results from two-dimensional wide-angle seismic modelling. Geophys. J. Int. 162:994–1006. https://doi.org/10.1111/j.1365-246X.2005.02710.x.
Maguire, P.K.H., Keller, G.R., Klemperer, S.L., Mackenzie, G.D., Keranen, K., Harder, S., O'Reilly, B., Thybo, H., Asfaw, L., Khan, M.A., Amha, M., 2006. Crustal structure of the northern Main Ethiopian Rift from the EAGLE controlled-source survey; a snapshot of incipient lithospheric break-up. In: Yirgu, G., Ebinger, C.J., Maguire, P.K.H. (Eds.), The Afar Volcanic Province Within the East African Rift System. Geological Society, London, Special Publications, London:pp. 269–292 https://doi.org/10.1144/GSL.SP.2006.259.01.21.
Mazzarini, F., Keir, D., Isola, I., 2013. Spatial relationship between earthquakes and volcanic vents in the central-northern Main Ethiopian Rift. J. Volcanol. Geotherm. Res. 262: 123–133. https://doi.org/10.1016/j.jvolgeores.2013.05.007.
Mickus, K., Tadesse, K., Keller, G.R., Oluma, B., 2007. Gravity analysis of the Main Ethiopian rift. J. Afr. Earth Sci. 48:59–69. https://doi.org/10.1016/j.jafrearsci.2007.02.008.
Mohr, P.A., 1962. Surface cauldron subsidence with associated faulting and fissure basalt eruptions at Gariboldi pass, Shoa, Ethiopia. Bull. Volcanol. 24:421–428. https://doi.org/10.1007/BF02599358.
Mohr, P.A., 1967. Major volcano-tectonic lineament in the Ethiopian rift system. Nature: 664–665 https://doi.org/10.1038/213664a0.
Mohr, P.a., 1971. Ethiopian rift and plateaus: some volcanic petrochemical differences. J. Geophys. Res. 76:1967–1984. https://doi.org/10.1029/JB076i008p01967.
Mohr, P., Mitchell, J.G., Raynolds, R.G.H., 1980. Quaternary volcanism and faulting at O'A caldera, central Ethiopian rift. Bull. Volcanol. 43:173–189. https://doi.org/10.1007/BF02597619.
Morbidelli, L., Nicoletti, M., Petrucciani, C., Piccirillo, E.M., 1975. Ethiopian South-Eastern Plateau and related escarpment: K/Ar ages of the main volcanic events (Main Ethiopian Rift from 8°10′ to 9°00′ lat. North). In: Pilger, A., Rosler, A. (Eds.), Afar Depression of Ethiopia. E. Schweizerbart'sche Verlagsbuchhandlung (Nägele u. Obermiller), Stuttgart, pp. 362–370.
Morgan, L.E., Renne, P.R., 2008. Diachronous dawn of Africa's Middle Stone Age: new $^{40}Ar/^{39}Ar$ ages from the Ethiopian Rift. Geology 36:967. https://doi.org/10.1130/G25213A.1.
Morton, W.H., Rex, D.C., Mitchell, J.G., Mohr, P., 1979. Riftward younging of volcanic units in the Addis Ababa region, Ethiopian rift valley. Nature 280:284–288. https://doi.org/10.1038/280284a0.
Muirhead, J.D., Kattenhorn, S.A., Le Corvec, N., 2015. Varying styles of magmatic strain accomodation across the East African Rift. AGU Publ. Geochem. Geophys. Geosyst. 16:2775–2795. https://doi.org/10.1002/2015GC005918.Received.
Nomikou, P., Parks, M.M., Papanikolaou, D., Pyle, D.M., Mather, T.A., Carey, S., Watts, A.B., Paulatto, M., Kalnins, M.L., Livanos, I., Bejelou, K., Simou, E., Perros, I., 2014. The emergence and growth of a submarine volcano: the Kameni islands, Santorini (Greece). GeoResJ 1–2:8–18. https://doi.org/10.1016/j.grj.2014.02.002.
Parnell-Turner, R., White, N., Henstock, T., Murton, B., Maclennan, J., Jones, S.M., 2014. A continuous 55-million-year record of transient mantle plume activity beneath Iceland. Nat. Geosci. 7:914–919. https://doi.org/10.1038/ngeo2281.
Peccerillo, A., Barberio, M.R., Yirgu, G., Ayalew, D., Barbieri, M., Wu, T.W., 2003. Relationships between mafic and peralkaline silicic magmatism in continental rift settings: a petrological, geochemical and isotopic study of the Gedemsa Volcano, Central Ethiopian Rift. J. Petrol. 44:2003–2032. https://doi.org/10.1093/petrology/egg068.
Piccirillo, E.M., Justin-Visentin, E., Zanettin, B., Joron, J.L., Treuil, M., 1979. Geodynamic evolution from plateau to rift: major and trace element geochemistry of the central eastern Ethiopian plateau volcanics. N. Jb. Geol. Paläont. (Abh.) 158 (2), 139–179.
Rapprich, V., Žáček, V., Verner, K., Erban, V., Goslar, T., Bekele, Y., Legesa, F., Hroch, T., Hejtmánková, P., 2016. Wendo Koshe Pumice: the latest Holocene silicic explosive eruption product of the Corbetti Volcanic System (Southern Ethiopia). J. Volcanol. Geotherm. Res. 310:159–171. https://doi.org/10.1016/j.jvolgeores.2015.12.008.
Ronga, F., Lustrino, M., Marzoli, A., Melluso, L., 2010. Petrogenesis of a basalt-comendite-pantellerite rock suite: the Boseti Volcanic Complex (Main Ethiopian Rift). Mineral. Petrol. 98:227–243. https://doi.org/10.1007/s00710-009-0064-3.
Rooney, T., Furman, T., Bastow, I., Ayalew, D., Yirgu, G., 2007. Lithospheric modification during crustal extension in the Main Ethiopian Rift. J. Geophys. Res. Solid Earth 112. https://doi.org/10.1029/2006JB004916.
Rooney, T.O., Bastow, I.D., Keir, D., Mazzarini, F., Movsesian, E., Grosfils, E.B., Zimbelman, J.R., Ramsey, M.S., Ayalew, D., Yirgu, G., 2014. The protracted development of focused magmatic intrusion during continental rifting. Tectonics 33:875–897. https://doi.org/10.1002/2013TC003514.
Rowland, J.V., Wilson, C.J.N., Gravley, D.M., 2010. Spatial and temporal variations in magma-assisted rifting, Taupo Volcanic Zone, New Zealand. J. Volcanol. Geotherm. Res. 190:89–108. https://doi.org/10.1016/j.jvolgeores.2009.05.004.
Sahle, Y., Hutchings, W.K., Braun, D.R., Sealy, J.C., Morgan, L.E., Negash, A., Atnafu, B., 2013. Earliest stone-tipped projectiles from the Ethiopian rift date to >279,000 years ago. PLoS One 8:1–9. https://doi.org/10.1371/journal.pone.0078092.
Sahle, Y., Morgan, L.E., Braun, D.R., Atnafu, B., Hutchings, W.K., 2014. Chronological and behavioral contexts of the earliest Middle Stone Age in the Gademotta formation, Main Ethiopian rift. Quat. Int. 331:6–19. https://doi.org/10.1016/j.quaint.2013.03.010.
Schilling, J., Kingsley, R.H., Hanan, B.B., Mccully, B.L., 1992. Nd-Sr-Pb isotopic variations along the Gulf of Aden: evidence for afar mantle plume - continental lithosphere interaction. J. Geophys. Res. 97, 927–966.
Sigmundsson, F., Hooper, A., Hreinsdóttir, S., Vogfjörd, K.S., Ófeigsson, B.G., Heimisson, E.R., Dumont, S., Parks, M., Spaans, K., Gudmundsson, G.B., Drouin, V., Árnadóttir, T., Jónsdóttir, K., Gudmundsson, M.T., Högnadóttir, T., Fridriksdóttir, H.M., Hensch, M., Einarsson, P., Magnússon, E., Samsonov, S., Brandsdóttir, B., White, R.S., Ágústsdóttir, T., Greenfield, T., Green, R.G., Hjartardóttir, Á.R., Pedersen, R., Bennett, R.A., Geirsson, H., La Femina, P.C., Björnsson, H., Pálsson, F., Sturkell, E., Bean, C.J., Möllhoff, M., Braiden, A.K., Eibl, E.P.S., 2015. Segmented lateral dyke growth in a rifting event at Bárðarbunga volcanic system, Iceland. Nature 517:15. https://doi.org/10.1038/nature14111.
Singer, B.S., Wijbrans, J.R., Nelson, S.T., Pringle, M.S., Feeley, T.C., Dungan, M.A., 1998. Inherited argon in a Pleistocene andesite lava: $^{40}Ar/^{39}Ar$ incremental-heating and laser-fusion analyses of plagioclase. Geology 26:427–430. https://doi.org/10.1130/0091-7613(1998)026<0427:IAIAPA>2.3.CO;2.
Sisson, T.W., Grove, T.L., 1993. Temperatures and H_2O contents of low-MgO high-alumina basalts. Contrib. Mineral. Petrol. 113:167–184. https://doi.org/10.1007/BF00283226.
Stamps, D.S., Calais, E., Saria, E., Hartnady, C., Nocquet, J.M., Ebinger, C.J., Fernandes, R.M., 2008. A kinematic model for the East African Rift. Geophys. Res. Lett. 35:1–6. https://doi.org/10.1029/2007GL032781.
Trua, T., Deniel, C., Mazzuoli, R., 1999. Crustal control in the genesis of Plio-Quaternary bimodal magmatism of the Main Ethiopian Rift (MER): geochemical and isotopic (Sr, Nd, Pb) evidence. Chem. Geol. 155:201–231. https://doi.org/10.1016/S0009-2541(98)00174-0.
Ukstins, I.A., Renne, P.R., Wolfenden, E., Baker, J., Ayalew, D., Menzies, M., 2002. Matching conjugate volcanic rifted margins: $^{40}Ar/^{39}Ar$ chrono-stratigraphy of pre- and syn-rift bimodal flood volcanism in Ethiopia and Yemen. Earth Planet. Sci. Lett. 198:289–306. https://doi.org/10.1016/S0012-821X(02)00525-3.
Vogel, N., Nomade, S., Negash, A., Renne, P.R., 2006. Forensic $^{40}Ar/^{39}Ar$ dating: a provenance study of Middle Stone Age obsidian artifacts from Ethiopia. J. Archaeol. Sci. 33:1749–1765. https://doi.org/10.1016/j.jas.2006.03.008.
Walker, G.P.L., 1999. Basaltic volcanoes and volcanic sytems. Encycl. Volcanoes.
Wendorf, F., Laury, R.L., Albritton, C.C., Schild, R., Vance Haynes, C., Damon, P.E., Shafiqullah, M., Scarborough, R., 1975. Dates for the Middle Stone Age of East Africa. Science (80-.) 187, 0–2.
Whaler, K.A., Hautot, S., 2006. The electrical resistivity structure of the crust beneath the northern Main Ethiopian Rift. In: Yirgu, G., Ebinger, C.J., Maguire, P.K.H. (Eds.), The Afar Volcanic Province Within the East African Rift System. Geological Society, London, Special Publications, London:pp. 293–305 https://doi.org/10.1144/GSL.SP.2006.259.01.22.
Williams, F.M., Williams, M.A.J., Aumento, F., 2004. Tensional fissures and crustal extension rates in the northern part of the Main Ethiopian Rift. J. Afr. Earth Sci. 38: 183–197. https://doi.org/10.1016/j.jafrearsci.2003.10.007.
WoldeGabriel, G., Aronson, J.L., Walter, R.C., 1990. Geochronology and rift basin development in the central sector of the Main Ethiopian Rift. Geol. Soc. Am. Bull. 102: 439–485. https://doi.org/10.1130/0016-7606(1990)102<0439.
Wolfenden, E., Ebinger, C., Yirgu, G., Deino, A., Ayalew, D., 2004. Evolution of the northern Main Ethiopian rift: birth of a triple junction. Earth Planet. Sci. Lett. 224:213–228. https://doi.org/10.1016/j.epsl.2004.04.022.
Wright, T.J., Ebinger, C., Biggs, J., Ayele, A., Yirgu, G., Keir, D., Stork, A., 2006. Magma-maintained rift segmentation at continental rupture in the 2005 Afar dyking episode. Nature 442:291–294. https://doi.org/10.1038/nature04978.